Chemical Science

ROYAL SOCIETY OF CHEMISTRY

REVIEW

View Article Online
View Journal | View Issue

Cite this: *Chem. Sci.*, 2021, **12**, 5044

Inorganic–inorganic nanohybrids for drug delivery, imaging and photo-therapy: recent developments and future scope

Goeun Choi,†[ab] N. Sanoj Rejinold,†[a] Huiyan Piao[a] and Jin-Ho Choy *[acd]

Advanced nanotechnology has been emerging rapidly in terms of novel hybrid nanomaterials that have found various applications in day-to-day life for the betterment of the public. Specifically, gold, iron, silica, hydroxy apatite, and layered double hydroxide based nanohybrids have shown tremendous progress in biomedical applications, including bio-imaging, therapeutic delivery and photothermal/dynamic therapy. Moreover, recent progress in up-conversion nanohybrid materials is also notable because they have excellent NIR imaging capability along with therapeutic benefits which would be useful for treating deep-rooted tumor tissues. Our present review highlights recent developments in inorganic–inorganic nanohybrids, and their applications in bio-imaging, drug delivery, and photo-therapy. In addition, their future scope is also discussed in detail.

Received 8th December 2020
Accepted 9th February 2021

DOI: 10.1039/d0sc06724e

rsc.li/chemical-science

1. Introduction

The biomedical field has been growing enormously to upgrade the standards and well-being of the public.[1] Specifically, biomedical nanotechnology, and diagnostic and therapeutic approaches have advanced dramatically due to recent significant developments in emerging theranostic materials.[2–7] However, they should be economic and affordable for everyone. There has been constant progress in the bio-engineering field, especially in the area of pharmaceutical sectors and drug-delivery agents. In particular, such progress reveals novel functional drug-delivery carriers capable of loading and delivering traditional chemo-agents with improved efficacy.[8] Such kinds of progress have helped the scientific community to come up with the term "nanomedicine" which is much better than traditional chemo-agents. Typically "nanomedicine" is a multi-disciplinary approach, which utilizes engineering as well as medical science to combat various diseases, such as cancer[9] and neuro-degenerative diseases.[10] The multi-disciplinary background of nanomedicine makes it very interesting and it basically comprises 6 major areas: pharmaceutical-drug delivery, bio-materials, diagnostics, drug development and therapy, *in vitro*/*in vivo* bio-imaging, and active bio-implants.

Recently, inorganic based nanohybrid materials, classified into inorganic–inorganic, organic–inorganic, and bio–inorganic nanohybrids, have shown improved benefits mainly due to their distinctive material properties. Such novel properties are hard to achieve by conventional solid-state reactions.[11–23] Therefore, in the emerging field of nanomedicine based on nanoscience and nanotechnology, it is very important to make advanced hybrid nanomaterials with specific properties with respect to their single/individual counterparts using synthetic methods like chemical vapor deposition, Langmuir–Blodgett technique, self-assembly, and intercalation reaction methods.[24–27] In the case of the latter, guest molecules are reversibly intercalated into 2-dimensional host lattices to form a variety of new nano–bio hybrids, such as inorganic–inorganic, organic–inorganic, and bio–inorganic hybrids with advanced properties.[28] It should also be noted that recent progress in nanochemistry has also helped to develop novel, creative multifunctional emerging nanohybrids simply by modifying the molecular re-arrangement of heterogeneously oriented organic–inorganic materials.[29–31] This novel, eccentric research field enable us to come up with a wide variety of nano–bio hybrid materials with already known/unknown properties which would be useful for drug delivery, bio-imaging and photo-therapy.

Since such nanohybrid materials have synergetic functionalities, this specific research area becomes very interesting for developing further intelligent hybrid materials. For instance, very highly photo-catalytic inorganic–inorganic nanohybrids could be developed *via* a simple exfoliation/restacking approach.[32] Several such approaches have been tried to develop novel functional nanohybrids based on inorganic-

[a]*Intelligent Nanohybrid Materials Laboratory (INML), Institute of Tissue Regeneration Engineering (ITREN), Dankook University, Cheonan 31116, Republic of Korea. E-mail: jhchoy@dankook.ac.kr*

[b]*College of Science and Technology, Dankook University, Cheonan 31116, Republic of Korea*

[c]*Department of Pre-medical Course, College of Medicine, Dankook University, Cheonan 31116, Republic of Korea*

[d]*Tokyo Tech World Research Hub Initiative (WRHI), Institute of Innovative Research, Tokyo Institute of Technology, Yokohama 226-8503, Japan*

† These authors contributed equally to this work.

chemical approaches: for example, nanoporous hybrids which can be utilized for both loading and releasing therapeutic agents.[33] This kind of hybrid approach of two or more inorganic materials has given birth to novel nanohybrids with potential multifunctional properties. Furthermore, by coupling multiple nanomaterials, the resulting hybrids are expected to possess better therapeutic efficacy than their individual counterparts.

Previously there were only a few reports on inorganic/organic nanohybrid materials and their bio-applications.[34,35] For example, Sreejith *et al.* (2015) reviewed nanohybrids for fluorescence, photo-acoustic and Raman bio-imaging applications.[35] On the other hand, inorganic–organic nanohybrid particles and their biomedical applications were reviewed as a book chapter by Katagiri (Elsevier Series on Advanced Ceramic Materials, 2021 edition).[36] Therefore, we believe that the present review would be the first on the specific topic of inorganic–inorganic nanohybrids and their biomedical applications. The actual purpose of this review is to give readers an insight into the overall outlook for nanohybrids: in particular, inorganic–inorganic nanohybrids and their specific uses in biomedical applications. We believe that this review would be helpful for understanding ongoing research in this emerging field, along with its advantages and limitations so that one can come up with a novel strategy for the betterment of human well-being in terms of clinical applications.

Therefore, the present review will detail trends in inorganic–inorganic nanohybrids that have been used for various biomedical applications, including drug delivery, bio-imaging and photo-therapy (Scheme 1). The term "inorganic–inorganic nanohybrids" is used only when there are two or three major inorganic components in the hybrid system. Drug molecules, such as DOX (doxorubicin) or PTX (paclitaxel), are considered here as model drugs, and stabilizing agents such as PEG, and targeting agents like folic acid (FA) or hyaluronic acid are considered as they are not in the mainstream of our current review. In addition, our review will specify applications and limitations associated with inorganic–inorganic nanohybrids along with future perspectives and scope.

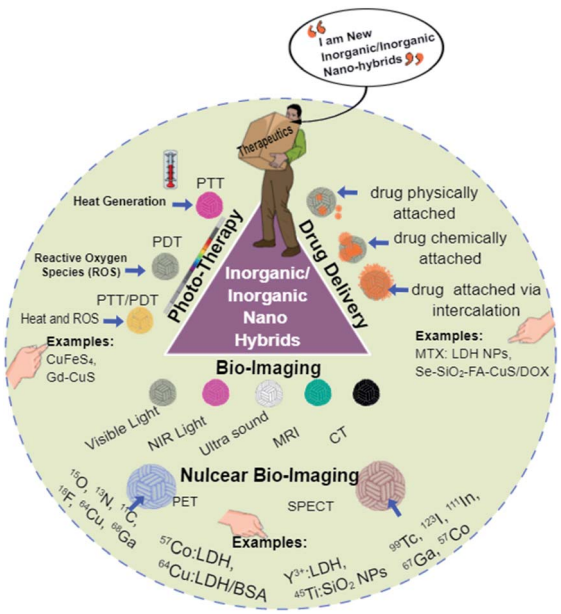

Scheme 1 Various inorganic–inorganic nanohybrids and their applications in drug delivery, bio-imaging and radio/photo-therapy.

2. Advantages of inorganic nanohybrids

Hybrid nanoparticles (NPs) are of great interest as they can have multiple properties when they are combined as a single moiety.[37] When individual molecules fail to give a specific function for a particular application, usually we prefer to combine them with a suitable molecule which can either boost, improve or impart a novel property to the nanohybrids. This is why they are very interesting for bio-applications including drug delivery[38,39] and bio-imaging.[40,41] Recently, there have been tremendous advancements in the inorganic nanoresearch area especially for biomedical applications. Nanohybrids of silica,[42] cobalt,[43] copper,[44] selenium,[45] ZnS,[46,47] iron[48] and layered double hydroxide NPs (LDH-NPs)[49] have been explored in order to achieve new properties. To exemplify this, generally LDH-NPs are acidically labile without having any specific therapeutic action; however, when they are intercalated with anionic drugs, LDH becomes an acidically degradable therapeutic functional molecule. In this way, hybridization helps to attain novel functionalities in a single material. In a similar way, LDH NPs have become useful for PET and SPECT-based imaging when they are hybridized with positron-emitting or gamma-emitting materials, as shown in Scheme 1. Pristine LDH NPs have no such properties until they are incorporated with these radioisotopes.

In addition, hybridization helps to improve the photo-stability and biocompatibility of QD materials as well. One such example is the shelling of comparatively toxic Cd–Se QDs with a biocompatible Zn–Te.[50] This kind of surface passivation not only improves biocompatibility, but it also helps to improve photo-stability as well. Such QD materials are far better than their single counterparts and have been used for bio-imaging applications.[50] CdTe/ZnTe nanohybrid QDs were also found to be non-toxic at the experimental dosage, proving that nano-hybridization has a positive impact on biocompatibility.[51]

Similarly, iron based NPs were hybridized with silica, in order to improve the biodegradability of the silica NPs, thereby improving their therapeutic applications.[52] There are many such studies exploring biomedical applications, including not only drug delivery, but tissue engineering applications as well.

In general, nanohybrids structures can combine multiple properties in a single structure. It is well known that hydroxy apatite (HAP) NPs are biocompatible and they have been explored for tissue engineering[53] and drug-delivery applications.[54] However, they do not have innate T1 contrasting properties. To implement this specific character, gadolinium (Gd) doping has been undertaken so that the new Gd-doped HAP will have a biodegradable nature along with T1 contrasting property in its hybrid structure.[53] In a similar way, Gd has been incorporated with rGO (reduced graphene oxide) in order to obtain

Table 1 Various inorganic–inorganic nanohybrid systems for drug-delivery applications

Specific application	Inorganic materials	Drug	Cell line/tumor model	Highlights	References
In vitro	Fe_3O_4/MSN	DOX	HeLa	Low cytotoxicity, efficient cell uptake ability on epithelioid human cervix carcinoma cell line (HeLa cells) and sustained drug release	60
	Au/HMSN	DOX	MCF-7	Controlled drug loading and releasing behavior. The NPs were well taken up by human breast cancer cell line (MCF-7 cells)	66
	CeO_2/MSN	Vitamin C/glutathione/ camptothecin	BxPC3	Controlled drug release and antioxidant behavior, highly reducing intracellular environment of cells. The *in vitro* proof of concept was done on the human pancreatic adenocarcinoma cell line (BxPC-3 cells)	85
	SiO_2/LDH	MTX	U20S	Good dispersibility, low cytotoxicity and effective inhibition of the human epithelial osteosarcoma cell line (U2OS cells)	94
	Fe_3O_4/LDH	DOX	HeLa	Biocompatible, effective inhibition of epithelioid human cervix cancer cell (HeLa cell) growth and magnetic hyperthermia cancer therapy	87
	Te/LDH/MSN	FA/paclitaxel	HepG2	Targeted chemo/PDT/PTT trimode combinatorial therapy on human liver hepatocellular carcinoma (HepG2 cells)	89
	ZnS:Mn/rGO	FA/DOX	MDA-MD-231	Improved media-dispersibility, drug loading/ release, tracking properties. The *in vitro* efficacy was tested on human mammary gland epithelial breast cancer cells (MDA-MB-231)	95
	Au/$MnFe_2O_4$	FA/DOX	Hep2	Non-toxic to normal cells and considerably toxic to human epithelial carcinoma (Hep2 cells), chemo- and magneto-hyperthermia	91
In vivo	Se/Au/$mSiO_2$	DOX	MDA-MB-231	Improved anti-tumor effects and delayed tumor progression in an *in vivo* human mammary gland epithelial breast cancer cell tumor model (MDA-MB-231) without causing any notable *in vivo* toxicity	93
	Se/CuS/MSN	DOX	HeLa	Enhanced targeting capability, synergistic chemo- (Se and DOX) photothermal therapy on epithelioid human cervix cancer cell (HeLa tumor) bearing mice	96
	Gd/MSN	Zoledronic acid/ plumbagin	MDA-MB-231 and 4T1	Early detection of bone-metastasis, and the proof of concept was established on a bone-metastatic breast cancer model (MDA-MB-231)	97
	LDH/MS	Curcumin	MCF-7 for *in vitro* and H22 for *in vivo*	Controlled drug release and great biocompatibility, enhanced antitumor effect against human breast cancer cells (MCF7) *in vitro* and anti-tumor efficacy was tested on a mouse liver cancer model	98
	BP/MSN	DOX	H22	Enhanced drug-loading capacity, high photothermal conversion efficiency and excellent release efficiency. The *in vivo* efficacy was studied using hepatoma (H22) bearing mice	99
	Fe_3O_4/WS_2/MSN	DOX	4T1	Low cytotoxicity, effective inhibition of tumor growth after combined photothermal and chemotherapy, as demonstrated on mouse mammary gland epithelial tumor (4T1) bearing mice	100

multiple properties, such as magnetic resonance imaging, optical coherence tomography and drug-delivery capability in their nanohybrid system.[55]

In general, we can say that nanohybrid materials improve physical/chemical stability, *in vivo* clearance, biocompatibility, and biodegradability to a large extent compared to their individual forms. Therefore, it is very important to have an overall understanding of such emerging and trending nanohybrids that have been explored recently for various biomedical applications.

3. Inorganic–inorganic nanohybrids for drug delivery

In recent years, designing drug carriers that have the ability to deliver drugs has received a lot of attention. Inorganic nanohybrids have provided a multi-purpose system for the transportation of a variety of anticancer and diagnostic agents.[56,57] Moreover, researchers have been working toward the development of inorganic–inorganic nanohybrids to provide drug-delivery systems (DDSs) that have great advantages over conventional carriers, such as improved drug-retaining ability, better pharmaco-kinetic properties, well-controlled release properties, and a targeted therapeutic approach.[58–60]

Here, some of the major developments and progress made in the drug-delivery area using inorganic nanohybrids, such as mesoporous silica NPs (MSNs), layered double hydroxides (LDHs), metal–organic frameworks (MOFs), metal NPs (*e.g.*, Au NPs, Ag NPs) and metal oxide NPs (*e.g.*, iron oxide (Fe_3O_4), cerium oxide (CeO_2), or manganese oxide (MnO_2)), will be discussed. In particular, characterizations of these nanocarriers are critical to controlling their desired behavior *in vitro* as well as *in vivo*, as described in Table 1.

3.1 *In vitro* study of inorganic–inorganic nanohybrids for drug delivery

Among the various materials employed in designing DDSs, MSNs have become a cynosure, owing to their physico-chemical characteristics, such as high surface area and large pore-volume along with their ability for functionalization.[61–65] It should be noted that their porous properties and structure are significantly governed by the synthesis background. Specific control over pore-diameter, topography, orientation and nanosize would help them to achieve selective adjustments to produce specific on-demand properties.[66] For example, Zhu's group developed an MSN-based hyperthermic, chemo-therapeutic DDS. This 150 nm sized bio-hybrid was based on Fe_3O_4, which was encapsulated within the MSNs, showing significant cellular localization without harming the cells.[67] The model drug DOX loaded magnetic MSNs showed significantly higher release at pH $\sim$ 5 than under neutral conditions, ensuring their tumor-responsive release properties, and could be beneficial for hyperthermia-mediated chemotherapy to treat a wide variety of cancers.[67]

In 2017, Li and coworkers successfully developed hollow MSNs (HMSNs) for drug-delivery purposes. Interestingly, these hollow cores can be controlled by a dual templating method by Au and cetyltrimethylammonium bromide (CTAB).[68] The hollow core tunability could also be able to control the DOX release pattern from HMSNs by changing the core size/thickness.

Chemo-radio-therapeutic targeted therapy based on Boron Neutron Capture Therapy (BNCT) is an emerging and useful technique to achieve selective tumor targeting with improved efficacy. Such efficacy is purely dependent on the type of tumor, intra-tumoral boron concentration and non-toxic absorption of thermal neutrons by boron.[69–71]

For example, Choy's group was successful in developing a new boron-delivering inorganic-nanohybrid system based on LDH for BNCT.[69] The as-made inorganic–inorganic nanohybrid mercaptoundecahydro-*closo*-dodecaborate (BSH)-LDH enhanced intracellular boron localization, thereby damaging the cancer cells effectively within a short irradiation time (Fig. 1A and B). The novel inorganic-nanohybrids enhanced BSH in tumor-to-blood significantly more than their counterparts (Fig. 1C).[69]

An economic strategy was used by Kaur *et al.* to prepare ^{10}BN nanohybrids using a simple solvo-thermal method. HeLa (epitheloid, cervix carcinoma, human origin), MCF-7 (human breast cancer cell line) cells were used to test its *in vitro* anti-tumor activity and it was shown that they are non-toxic anti-cancer agents.[70] Typically, a few inorganic-based therapeutic agents are briefly reviewed from a chemical point of view. Platinum-based therapeutic agents, such as cisplatin,[72] carboplatin[73–75] and oxaliplatin,[76–78] and a ruthenium(III) complex[79] have been well explored in the drug-delivery field.

For example, Lin *et al.* developed a novel cisplatin (CP) delivery system by the modification of mesoporous silica nanoparticles (MSNs) through carboxyl functionalization.[80] This inorganic–inorganic nanohybrid might be advantageous for sustained release and less hydrolytic degradation *in vivo*. A similar study was reported by Kannan *et al.*, where their research group developed cisplatin/silica hybrids for sustained drug-delivery applications.[81]

Similarly, magnetically targeted silica-nanohybrids were developed for cisplatin release based on magnetic hyperthermia under mild conditions.[82] Dumbbell-shaped Au–Fe_3O_4 nanohybrids were developed with enhanced target-specificity to deliver platin into Her2-positive breast cancer cells with better therapeutic benefits than the free cisplatin molecule.[83] A ruthenium-based complex with $mSiO_2$ NPs was developed as a pH-sensitive drug-delivery agent to achieve the controlled release of Ru(II) to cancer cells without causing adverse effects on normal cells.[84]

There has been huge progress in the ceria (Ce)-based hybrid NP field as well, especially due to their antioxidant properties. For example, Zhu's group developed an antioxidant-sensitive therapeutic system consisting of redox-susceptible CeO_2 NPs.[85] The therapeutics-loaded CeO_2-covered MSNs under vitamin C/GSH conditions help the coated CeO_2 NPs to undergo rapid degradation, allowing the MSN pores to release the payload effectively. Preliminary studies using *in vitro* experiments showed that this proof of concept could be extended to further applications.

Another notable advancement can be observed in the LDH research area. Besides their well-known biocompatibility, and biodegradability, they are highly economic and easy to modify with other functional materials, making them a perfect inorganic candidate for hybridizing with various clinically relevant materials. In addition, their anion exchange capability, pH responsivity, and cell-penetrability along with endosomal escape are also noticeable.[68,86,87] For example, Li *et al.* used a nanodot-coating technique to make (10–15 nm) sized SiO_2 dot-coatings on the LDH (110 nm) to finally achieve 170 nm

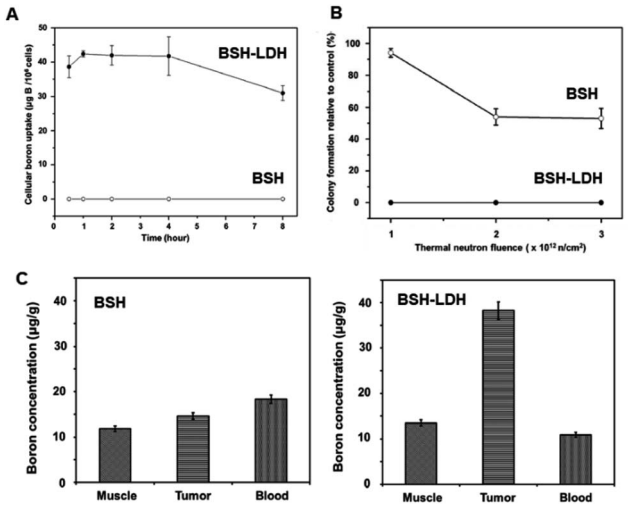

Fig. 1 (A) Cellular boron uptake of BSH and BSH-LDH in the U87 glioblastoma cell line. (B) Colony formation ability for BSH-LDH-treated U87 cells and BSH-treated cells after thermal neutron irradiation. (C) Bio-distribution studies of boron in each tissue of U87 xenograft tumor-bearing mice treated with BSH and BSH-LDH for 2 h after administration.[69] Reproduced from ref. 69 with permission from Wiley-VCH Verlag GmbH & Co. KGaA, copyright 2018.

sized (SiO_2@MgAl-LDH) nanohybrids. The as-made nanohybrids were well-dispersible with an optimum size range for drug-delivery applications[88] (Fig. 2A). Methotrexate (MTX) was loaded on these nanohybrids, showing efficient cellular uptake on human osteosarcoma cells, inhibiting cancer cell growth (Fig. 2B). In addition, the new nanohybrids were non-toxic at an LDH concentration below 200 μg mL^{-1} (Fig. 2C).[88]

Similarly, a combined magneto/thermo/chemo therapy strategy was tested using Fe_3O_4/LDH nanohybrids.[89] The as-made nanohybrids showed a significantly high DOX loading capability and good cytocompatibility on tested cell lines, such as L929 and HeLa cell lines, respectively. The magnetic hyperthermia experiments revealed that they are potent agents for such applications.

Carbon-based NPs such as graphene oxide (GO) and reduced graphene oxide (rGO) have been used as biomedicines too.[90,91] Their exceptional physico-chemical and mechanical properties have allowed single-layered graphene to be used as a novel nanocarrier for drug and gene delivery. For instance, Diaz-Diestra *et al.* developed a nanohybrid comprised of rGO/Mn:ZnS QDs further coated with folic acid to form FA-rGO/ZnS:Mn[92] The DOX was attached on the graphene *via* π–π stacking, in addition to hydrophobic interaction. The 35% entrapment and 60% loading efficiency were associated with DOX chelation to Zn^{2+}. These targeted inorganic nanohybrids clearly showed that active targeting is a better strategy to treat cancer cells efficiently.

Similarly, another targeted approach was made using $MnFe_2O_4$@Au nanohybrids for DOX delivery *via* FA-mediated targeted therapy.[93] The as-made $MnFe_2O_4$@Au–FA–DOX nanohybrid showed selective toxicity only to Hep2 cells without harming normal cells under magnetic hyperthermia conditions, clearly showing these novel multifunctional active nanohybrids would be very effective for magnetic hyperthermia-mediated apoptosis.

3.2 *In vivo* study of inorganic–inorganic nanohybrids for drug-delivery applications

Pre-clinical evaluation of biomaterials is very important before considering them as clinically relevant biomaterials. Therefore, newly developed nanohybrids should also undergo various *in vivo* studies which are basically related to their pharmaco-kinetic and pharmaco-dynamic evaluation. Even though many researchers could successfully demonstrate the potency of their developed NPs *in vitro*, only a few were able to translate such *in vitro* studies into *in vivo* success. For any kind of functional biomaterial, it is important to have excellent biocompatibility, blood compatibility, serum stability, and *in vivo* clearance from the body without causing any damage to the vital organs. Therefore, understanding the *in vivo* fate of newly developed nano–bio hybrids should be of utmost priority in clinical perspectives.

Qiao *et al.* developed a pH-sensitive bone-targetable therapeutic agent based on zoledronic acid (ZA) which was anchored on $mSiO_2$/Gd(III) UC (up-conversion) nanohybrids. These materials encapsulated plumbagin (PL) for bone metastasis at an early stage.[97] The *in vivo* analysis using a cancer bone metastasis model proved their efficacy since there was an effective reduction in osteo-clastogenesis and tumorigenesis.

Cao *et al.* developed a pH-responsive nanocarrier based on LDH modified with $mSiO_2$ to form LDH@$mSiO_2$ with a thickness of 9 nm.[98] The outer silica coating significantly enhanced nanohybrid stability. Besides that, it showed pH sensitivity because of silica degradation in acidic conditions. The curcumin-encapsulated nanohybrids showed improved anti-

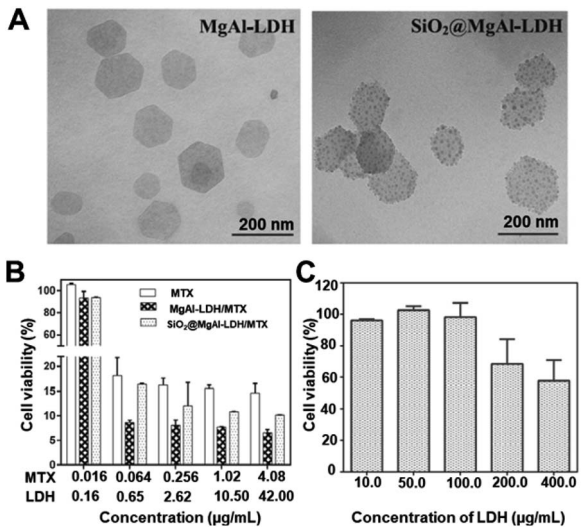

Fig. 2 (A) TEM images of MgAl-LDH and SiO_2@MgAl-LDH nanocomposites. (B) MTT assay analysis of the effects of MTX treatments delivered by MgAl-LDH and SiO_2@MgAl-LDH. (C) Cytotoxicity of SiO_2@MgAl-LDHs at different concentrations to U2OS cell lines. The cell viability of U2OS exposed to different amounts of MTX associated with or without MgAl-LDH and SiO_2@MgAl-LDH for 72 h.[88] Reproduced from ref. 88 with permission from Elsevier Ltd, copyright 2016.

cancer efficacy towards mammary cancer cells, which was translated into *in vivo* experiments as well. This study clearly showed that LDH-based nanohybrids would be economic and reliable therapeutic agents for cancer therapy. The preliminary studies open up new possibilities for engineering better and more efficient therapeutic DDSs with enhanced outcomes.

4. Inorganic–inorganic nanohybrids for bio-imaging

A variety of inorganic–inorganic nanohybrids have been developed recently for bio-imaging, including optical (visible, IR, NIR, NIR-II), magnetic resonance imaging (MRI), X-ray, nuclear and photo-acoustic imaging (PAI). In particular, NIR and PAI have advanced significantly with inorganic–inorganic nanohybrid materials.

4.1 Inorganic–inorganic nanohybrids as optical imaging agents

There are various diagnostic tools currently available in the medical field, including optical imaging techniques such as UV, IR, NIR-I and NIR-II based, MRI, PET and SPECT, which vary in their sensitivity and spatial resolution.[101–103] For example, while PET and SPECT, which are based on radioisotopic element-doped nanohybrids, show good sensitivity, they have lower resolution (~1–2 mm), making it hard for an effective diagnosis for certain tumors. Similarly, optical imaging techniques (UV, IR) also have limitations as they have low spatial resolution (2–3 mm) limiting their penetration towards certain solid tumors (depth of <1 cm), but they have nevertheless been widely accepted as imaging techniques, especially for studying the *in vitro* cellular-trafficking of various bio-fluorescent materials, mainly due to their being economic and effective in such *in vitro* experiments. Recent developments in optical imaging agents using inorganic–inorganic nanohybrids are listed in Table 2.

Typically optical imaging techniques utilize light from the visible region to the NIR (I & II) and have been widely utilized in *in vitro*/*in vivo* analysis, as mentioned before. This is mainly because of their high sensitivity, real-time trafficking ability, and of course low cost. Their basic limitations include scattering with low resolution along with low permeability. In addition to these, auto-fluorescence is also a limitation associated with optical imaging, especially under *in vivo* conditions, where adjacent tissues, lipids or water molecules can lead to such auto-florescence conditions.[102–104] Nonetheless, this imaging strategy is beneficial for effectively studying newly developed nano–bio hybrids and their cellular interactions, mainly because such sub-cellular level interactions could be visualized only *via* an optical imaging strategy.[101,105,106] There has been a wide variety of optical imaging agents, mostly based on cyanine-based dyes, such as cyanine-5.5 (Cy5.5), FITC, and rhodamine B iso-thiocyanate (RITC). Typically, inorganic nanohybrids are utilized to load such dye molecules into their lattice layers, in particular for LDH NPs. An intercalation technique has been widely used to make such nanohybrids.[105,107] Chemical conjugation techniques are also well accepted for making inorganic-hybrids, where such dye molecules can easily be attached onto the surface through specific reaction strategies like the silane-coupling reaction.[106,108]

For example, Choy *et al.* developed an *in vivo* method along with *in vitro* cell localization studies of FITC-LDHs and RITC-LDH.[105,106,109,110] As represented in Fig. 3, FITC moieties are well attached on the LDH lattice-layers, forming an effective nanohybrid (FITC-LDH) (Fig. 3A). *In vitro* studies using tumorigenic osteosarcoma MNNG/HOS cell treated samples visualized improved fluorescent signals within the cells in a 2 h inoculation period (Fig. 3B). The FITC-LDH got into the cell through

Table 2 Summary of layered metal hydroxides for optical imaging

Optical imaging functions	Composition of materials	Imaging agent	*In vitro*/*in vivo* highlights	Reference
Fluorescent images	MgAl-FITC-LDH	FITC	Investigation of intercellular uptake mechanism for LDH nanovehicles using an MNNG/HOS osteosarcoma cell line	105
Fluorescent images	MgAl-FITC-LDH	FITC	Investigation of intracellular trafficking pathway for an LDH nanovehicle using an MNNG/HOS osteosarcoma cell line	109
Fluorescent images	MgAl-FITC-LDH	FITC	Drug-delivery carriers with a targeting function due to the chemical conjugation with a specific ligand	119
Fluorescent images	MgAl-FITC-LDH MgAl-RITC-LDH	FITC RITC	*In vitro* or *in vivo* biocompatibility of LDH nanovehicles was evaluated on an MNNG/HOS osteosarcoma cancer model *in vivo*	110
SPECT	^{57}CoMgAl-LDH	^{57}Co	^{57}Co-LDH NPs showed effective cellular uptake behaviour *in vitro*, which was proved by *in vivo* using a mouse colorectal cancer cell line, CT-26 tumor bearing mouse model	120
PET	^{64}CuMgAl-LDH-BSA	^{64}Cu	LDH NPs labelled with PET radioisotopes were selectively accumulated in tumor tissues *via* a passive targeting effect using a mouse mammary gland cancer cells line, 4T1 tumor model	121

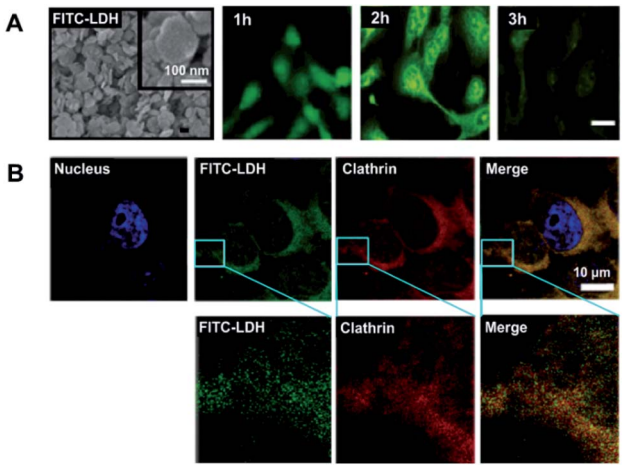

Fig. 3 (A) SEM representation of FITC-LDH; and intra-cellular time-dependent localization studies on FITC-LDH-treated MNNG/HOS cells, and (B) confocal microscopic images showing co-localization by FITC-LDH and clathrin in MNNG/HOS cells. Cells are treated with FITC-LDH for 2 h, incubated with clathrin antibodies, followed by Texas Red/DAPI staining.[105] Reproduced from ref. 105 with permission from the American Chemical Society, copyright 2006.

a clathrin-mediated pathway, as shown in Fig. 3B. The results clearly show the cell-penetrating capability of LDH-based novel inorganic nanohybrids, and their low cellular toxicity makes them an effective bio-template for making a wide variety of inorganic–inorganic nano–bio hybrids.[105,106,109,110]

This kind of study is very promising and interesting because such LDH-nanohybrids could be developed into inorganic–inorganic molecular structures for bio-imaging purposes. For example, various inorganic–inorganic nanohybrids, such as Au/ZnO,[111] ZnO/Mn,[112] and CdTe/ZnTe nanohybrids,[51] were developed in order to improve photo-stability and thereby imaging capability *in vitro* and *in vivo*.

It is well known that most fluorescent dye molecules easily undergo bleaching, thereby limiting their applications, and they need a photo-stabilizer to protect them in a biocompatible polymer matrix. In contrast, inorganic–inorganic nanohybrid based optical imaging agents are very important as they can significantly improve optical-imaging properties (for example, CdSe:ZnTe QDs[113]). There has been constant progress in inorganic-based fluorescent dyes where a doping strategy is used to make such hybrid materials. For example, LDH NPs have been doped with lanthanide elements in order to achieve effective bio-imaging.[114] The f–f, f–d electron transitions in the lanthanide series achieve such an optical imaging capability when they are doped into 2D inorganic LDH NPs. In addition, the lanthanide series has long fluorescence along with a Stokes shift with improved photo-stability.[115] To realize this, a significantly improved fluorescent inorganic-based fluorescent dye was developed with MgAl-LDH on doping with Tb^{3+} ions.[116] A similar trend was observed when Eu^{3+} was doped into Zn–Al-LDH (λ_{em} = 520–720 nm) *via* a $^5D_0$–^7D_J (J = 1–4) Eu^{3+} transition.[117] Although these Ln^{3+} hybrids showed better luminescence properties, there are still drawbacks mainly due to the quenching effect as they are co-ordinated *via* the hydroxyl groups with Ln^{3+} metallic centres, limiting their long-term applications. In order to compensate for such issues, generally organic UV sensitizers can be attached which can convert light into Ln^{3+} excitons.[116] Such kinds of studies have been undertaken by Liu *et al.* where a combined doping of Tb^{3+} and Gd^{3+} along with LDH intercalation was undertaken, boosting the multiple energy transfer channels.[118] Exfoliated LEuH (layered europium hydroxide)-fluorescent molecule HPTS (8-hydroxy-pyrene-1,3,6-trisulfonate) was reported by Gu *et al.*, showing good photo-stability, high absorbance with a high quantum yield, *etc.* The observed blue luminescence at 440 nm found in formamide (FM) was associated with synergies such as electrostatic interaction through LEuH layer-anionic HPTS and hydrogen bonding within HPTS–FM. Besides that, there was Eu^{3+}–HPTS energy-transfer *via* the excited state proton transfer (ESPT) process.[114] These initial studies clearly show that such novel inorganic-nanohybrids with targeting moieties would be effective for improving the optical imaging properties of a wide variety of chemically modified inorganic–inorganic hybrid structures with improved photo-stability for long-term applications.

Even though the optical imaging strategies are really beneficial for inter/intra-cyto localization and studying intra-cyto pathways, along with pharmaco-kinetic mechanisms such as *in vivo* distribution, bio-accumulation and clearance of nanoparticles and hybrid materials, an imaging agent is still required for modifying the surface of inorganic-biomaterials through surface-functionalization methods. We should also clearly understand the electronic structure and PL characteristic of lanthanide^{3+} ions for developing novel LDH-based inorganic–inorganic nanohybrids by tuning their chemical structure for improved theranostic applications, including imaging-guided therapeutic strategies.

It is well known that organic fluorochromes are necessary for *in vitro*/*in vivo* imaging. However, this dependency on organic molecules could be avoided by making novel inorganic–inorganic nanohybrids that have tunable opto-electronic properties. For example, deep-rooted *in vivo* tissue imaging is possible with NIR-responsive gold/silica nanohybrids.[122]

Similarly, recent developments in up-conversion materials give us hope that we can completely depend upon novel inorganic–inorganic nanohybrids for safer optical imaging under *in vitro*/*in vivo* conditions.

4.2 Inorganic–inorganic nanohybrids as magnetic imaging agents

There have been various developments in improving MRI contrasting agents with high resolution. Currently available MRI agents have serious disadvantages as they are complexed with organic chelating agents which could leach out the Gd ions and could be detrimental to the human body. Therefore, novel inorganic–inorganic MRI agents are necessary for their eligibility as next-generation MRI agents.

With this context, there have been various progressive pieces of research, in particular for iron-based inorganic nanohybrids. For example, silica-coated superparamagnetic iron oxide NPs were developed as better T1-weighted MRI agents. 30–40 nm sized superparamagnetic iron oxide nanoparticles (SPIONS)

showed improved T1 magnetic resonance spectroscopy (MRS) *in vivo* after intravenous injection (i.v.) using an animal model.[123]

Zn^{2+}-doped Fe_3O_4 core/mesoporous silica nanohybrids were developed for MRI enhancement and tumor-targeted agents. *In vitro* studies clearly demonstrated their MRI imaging capability as T2-weighed contrasting agents.[124]

4.3 Inorganic–inorganic nanohybrids as photo-acoustic imaging agents

In 1880, Alexander Graham Bell introduced photo-acoustic imaging (PAI), and from then on PAI has been emerging progressively as a promising imaging agent based on the PA effect.[125] This imaging technique can provide detailed real-time information with high spatial resolution[126] on the anatomical, functional and molecular level of pathogenic tissues without using ionizing radiation.[127,128] In addition, it has higher spatial resolution (as low as 5 μm) than fluorescence optical imaging, along with a deeper imaging depth (up to 5–6 cm).[126] This is because it uses the low scattering effects of ultrasonic signals rather than light in pathogenic tissues. In addition, it is non-ionizing and characterized by deep tissue contrasting properties.

Au-NPs have been widely used as a PA contrasting agent mainly due to their surface plasmon resonance effects.[126] In addition, various inorganic–inorganic nanohybrids have been reported for similar applications. For example, graphene oxide modified Au–SiO_2 core–shell nanohybrids were developed for PA signal generation and bimodal imaging *via* PA and fluorescence.[129] Similarly, gold/silica nanohybrids were tested for their *in vivo* PAI effects by Park *et al.* (2018).[130] Unlike other inorganic hybrid NPs, these coating- or stabilizer-free nanohybrids show unbelievable improvements *in vivo*, which should be understood and well studied for further clinical applications.

4.4 Inorganic–inorganic nanohybrids as nuclear imaging agents

In 1896, the prominent scientists Becquerel and the Curies introduced radium and opened up a Pandora's Box, enabling a wide variety of possibilities in the radio-research field. One such research field is the development of nuclear medicine and nuclear imaging. The latter was produced by the gamma camera, invented by Anger (1958), to detect tomographical features of living tissues in the form of SPECT or PET[131] with very high detection sensitivity, in the concentration range of 10^{-9} to 10^{-12} M.[131]

In SPECT, imaging agents or carrier molecules are generally doped with a wide variety of gamma-emitting radioisotopes such as ^{99m}Tc, ^{123}I, ^{111}In, ^{67}Ga or ^{57}Co. In contrast, PET utilizes positron-emitting radioisotope labeled nanomaterials for detection analysis. PET agents include radionuclides such as ^{15}O, ^{13}N, ^{11}C, ^{18}F, ^{64}Cu and ^{68}Ga.[132] Typically, such SPECT-imaging agents are administered into the body through intraperitoneal injection (i.p.) or i.v. so that the images can be obtained from γ-rays generated from the radioactive imaging agents inside the body. To exemplify this phenomenon, ^{18}F can be shown as: ${}^{18}_{9}\mathrm{F} \rightarrow {}^{18}_{8}\mathrm{F} + {}^{0}_{1}\beta(\text{positron}) + \nu_e(\text{neutrino})$. This emitted positron comes into contact with an electron from adjacent surroundings right after a short distance of travel; then those two particles "annihilate" to produce γ-rays (511 keV) in opposite directions. These γ-rays are e-detected for PET imaging through a reconstruction strategy using software. It should be noted that such radioisotopes do not bear any tumor-homing capability, apart from iodine ones (^{123}I, ^{124}I, ^{125}I, and ^{131}I for SPECT, PET, and radiotherapy). This could be mainly because of the targeting nature of iodine towards the thyroid. Iodine is an important chemical for thyroid hormonal function; therefore, iodinated inorganic–inorganic nanohybrids would be a useful radiotherapeutic strategy to treat various types of thyroid malignancies. Therefore, radioisotopes need to be incorporated or bound with a chemically stable carrier to be transferred to the target area.[120]

As mentioned before, incorporating such radioisotopic materials into the lattice layers gives birth to a wide variety of nano–bio hybrids for theranostic applications. To make nuclear imaging agents, therefore, the incorporation of radioisotopes, including ^{57}Co, ^{64}Cu, ^{67}Ga and ^{68}Ga, has been reported owing to their excellent chemical stability with improved biocompatibility in *in vivo* conditions.[120] Previously there have been reports for making radioisotope-labeled LDHs, where ^{57}Co and ^{67}Ga are directly incorporated into the LDH lattice.[133] ^{57}Co-labelled-LDH (Co-57/LDH) was successfully synthesized *via* hydrothermal substitution reaction reported by Kim, along with biological assessment on mouse colon carcinoma cell cells (CT-26) and human hepatocellular carcinoma cells (HepG2) showed promising results both *in vitro* and *in vivo*. The *in vivo* PK studies on bio-distribution assessment using a CT-26 xenograft model using a BALB/c mice model showed that such hybrids based on radioisotope-labeled LDHs could be a potential delivery carrier for inducing radioactivity at the tumor site.[120]

Another study by Shi *et al.* showed that LDHs when coated with BSA and labeled PET radioisotopes (^{64}Cu, ^{44}Sc, and ^{89}Zr) (Fig. 4A) were able to produce very high resolution PET images, as demonstrated by animal studies using a 4T1 mouse tumor xenograft model. The ^{64}Cu-LDH-BSA hybrids were well localized into the 4T1 tumor mainly through the EPR effect, confirming their targetability (Fig. 4B).[134] Such kinds of 2D-inorganic nanohybrids with radio-labelling strategies are quite interesting, though they are in the early stages. New nano–bio hybrids materials are on the way to improve the current limitations associated with 2D hybrids.

In another study, 150 nm sized silica NPs were radio-labeled with ^{45}Ti to impart PET. The *in vivo* results on 4T1 tumor models showed that these nanohybrids were effective for PET imaging.[135] Similarly, a chelator-free approach has been adopted for developing ^{89}Zr-labelled silica NPs for PET-guided drug-delivery applications. Compared to traditional chelator-based nano-approaches, these new nanohybrids would improve the long-term *in vivo* integrity along with better stability. These developed nanohybrids showed 20 day long-term *in vivo* stability, confirming their suitability as a good PET imaging agent (Fig. 5).[136]

It should be noted that simple mixing of radioisotopes with LDHs results in low labelling yield and thereby poor stability. This could be because of the low chemical interaction of radioisotopes with the LDH surface. Therefore, one has to think of an appropriate research strategy to compensate for such

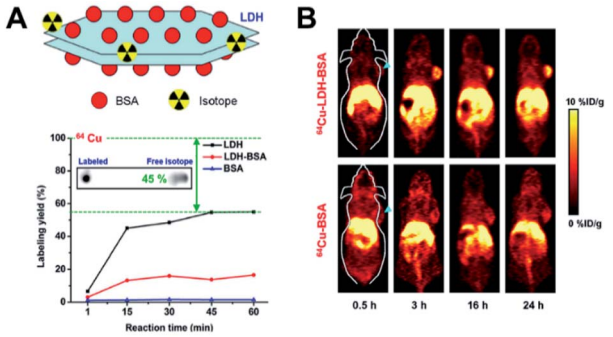

Fig. 4 (A) ^{64}Cu-LDH-BSA schematic representation, autoradiographic images of TLC plates of chelator-free labeled-64Cu LDH for 1 h, with a labeling yield of LDH, LDH-BSA and BSA after chelator-free labeling with ^{64}Cu at different reaction times calculated from autoradiography images of TLC plates and (B) post-injection, time-dependent PET images for ^{64}Cu-LDH-BSA and ^{64}Cu-BSA on 4T1 tumor-bearing mice. Strong tumor signals observed in the mice post-injection with ^{64}Cu-LDH-BSA.[134] Reproduced from ref. 134 with permission from Nature Publishing Group, copyright 2015.

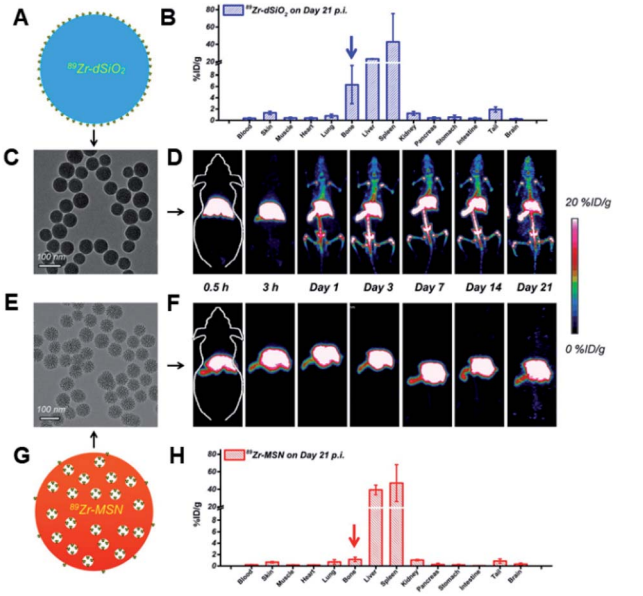

Fig. 5 *In vivo* radio-stability and *ex vivo* bio-distribution studies. (A) Schematic representation for ^{89}Zr-dSiO$_2$. (B) Bio-distribution study of ^{89}Zr–dSiO$_2$ on day 21 p.i (post injection). (C) TEM image of ^{89}Zr–dSiO$_2$. (D) *In vivo* serial coronal maximum intensity projection PET images of mice at different time points after i.v. injection of ^{89}Zr–dSiO$_2$. (E) TEM image of ^{89}Zr–MSN. (F) *In vivo* serial coronal maximum intensity projection PET images of mice at different time points after i.v. injection of ^{89}Zr–MSN. (G) Schematic illustration of ^{89}Zr–MSN. (H) Bio-distribution study of ^{89}Zr–MSN on day 21 p.i.[136] Reproduced from ref. 136 (https://pubs.acs.org/doi/10.1021/acsnano.5b00526) with permission from the American Chemical Society, copyright 2015.

limitations for better imaging techniques. Immobilization of radioisotope on the LDH surface is another strategy to overcome the limitations mentioned here. For example, recently Eom *et al.* demonstrated the successful synthesis of Y-LDH, where Al^{3+} ions in an LDH lattice were isomorphically substituted with Y^{3+} ions, hoping to develop such a proof of concept in real applications in radiotherapy.[137] However, more research is required to expand the possibility of radioisotope-labeled LDH-based inorganic nano–bio hybrids with very good chemical and physical stability not just for imaging purposes, but for simultaneous radiotherapy as well. Finding a proper synthetic method with high biocompatibility with excellent radio-labelling capacity would be highly preferable for use of such materials for real application purposes.

We expect that 2D nanomaterials could play a vital role as an excellent nuclear biomedicine, owing to their significantly high radio-labeling efficiency and chemical stability. To be utilized further as better nuclear medicines, it is important to study their *in vitro* and *in vivo* toxicity profiles in detail. Therefore, pre-clinical analysis on long-term toxicity and detailed pharmacokinetics and bio-accumulation and their impact on the human body *etc.* should be well understood in order to fully utilize such radio-labelled inorganic nanohybrids. Safety, accumulation in the body and clearance from the circulation *etc.* are very critical prior to any clinical analysis. We believe that such precise and accurate information could help us to realize LDH as "excellent nuclear nanomedicine" sooner or later.

5. Inorganic–inorganic nanohybrids for photothermal and photodynamic therapies with imaging properties

Photo-therapy uses photo-energy to convert it into heat of reactive singlet oxygen species which can have significant therapeutic benefits on malignant cells/tissues. Photo-therapy mainly consists of two approaches, PTT (photothermal therapy) and PDT (photo-dynamic therapy), and a combination of PTT/PDT, which is also widely used for treating various malignancies (Table 3).

5.1 Inorganic–inorganic nanohybrids for combined PTT/Imaging applications

Inorganic–inorganic nanohybrids include metals, alloys, and composite-based nanohybrids for photo-therapy.[138,139] A main focus will be on recent developments within the last 5 years. Gold and iron metal-based nanohybrids have already been well explored in this field. New materials include LDH-based composites for such applications. The future scope and clinical perspectives of such inorganic–inorganic nanohybrids will be detailed in this section.

Selective tumor targeting of plasmonic materials along with multimodal imaging strategies are the key to a successful photo-thermal treatment.[140] A nanohybrid multi-potent system was made using iron oxide/gold (Fe_2O_3/Au) core–shell NPs to realize the above-mentioned goals. The Au shell was meant for PTT, while MRI was enabled by the Fe_2O_3 core along with localized drug targeting through the iron core, enabling direct effective accumulation of these nanohybrids into the tumor region. Intravenously injected Fe_2O_3@Au on BALB/c mice bearing a CT26 colorectal tumor model was exposed to a magnet for 3 h to locate the NPs, followed by near infrared (NIR) laser irradiation. Intratumoral accumulation of these NPs

Table 3 Various inorganic–inorganic nanohybrid systems for photo-therapy applications

Specific application	Materials	Highlights	Remarks	Ref.
PTT	Iron oxide/gold core–shell nano-nanohybrids	Magnetic core with an average diameter of 22 nm and Au shell with ~5 nm thickness uniformly covers the magnetic core. The hydrodynamic diameter of Fe_2O_3@Au measured by DLS shows that the effective diameter of the NPs is ~37 nm	Improved magnetically targeted thermotherapy against a BALB/c mice bearing a CT26 colorectal tumor model	140
PTT	Silica/gold with a thermo-sensitive gel	For imaging-guided interventional therapy in patient-derived xenograft of pancreatic cancer	Imaging-guided interventional therapy, clinical thinking of surgical resection and postoperative chemotherapy, single administration and exemption from repeated punctures, no recurrence, multimodality imaging and omnidirectional treatment	143
PTT	Co–P/MnO_2/mSiO_2	MRI-guided effective PTT	Dual modal T1/T2 MRI-guided effective PTT along with pH sensitivity and demonstrated on a 4T1 (mouse mammary gland, epithelial cancer cell line) bearing mouse model	142
PTT	Se@SiO_2–FA–CuS nanohybrids	Size-Se@SiO_2 nanospheres had a uniform size of about 66 (composite particle size was not mentioned) zeta-Se@SiO_2–FA–CuS/DOX (19.2 mV). Since the loaded DOX has fluorescence, it can be used for cellular imaging purposes.	Improved chemo-thermotherapy against epithelioid human cervix carcinoma cell line (HeLa cells)	144
PTT	Gold nanostar-coated hollow mesoporous silica	All in one for (1) ultra sound (US), (2) PTT, (3) CT and (4) PAI	Improved efficacy on a C6 (rat glioma cell line) tumor model.	145
PTT	Iron-doped copper sulfide hybrid NPs ($CuFeS_4$)	(PA) imaging and PTT, MRI	Cu_5FeS_4-PEG exhibits a high tumor uptake (~10% ID g^{-1}) after intravenous injection. *In vitro* and *in vivo* cancer treatment further confirmed that Cu_5FeS_4-PEG could act as a novel therapeutic agent for PTT towards a mouse mammary gland cancer cell line, 4T1 tumor bearing mouse model	146
PTT	Reduced graphene/Au nanostars	Effective killing of micro-organisms (bacteria) – methicillin-resistant *Staphylococcus aureus* (MRSA)	Significant enhancement in bactericidal efficiency, (complete death) by hyperthermic effect of rGO/AuNS	147
PTT/PDT	Gd oxide–gold nanoclusters hybrid	Simultaneous PTT/PDT/CT/NIRF/MRI	*In vivo* therapeutic studies are not given, though they showed triple modal imaging *in vivo*	148
PTT/PDT	Ultrasmall MoS_2 nanodot-doped biodegradable SiO_2 nanoparticles hybridized with Clorin-e6 (Ce6) and HA	Clearable FL/CT/MSOT imaging-guided PTT/PDT combination tumor therapy against a mouse mammary gland cancer cell line, 4T1 tumor bearing mouse model	Detailed toxicity of such NPs is not given in the manuscript	149
PTT	$NaBiF_4$: Gd@PDA@PEG nanomaterials	Real-time temperature *in vivo* monitoring for MR-guided imaging	*In vivo* toxicity is needed for such composite nanohybrids	150
PTT	Albumin–Gd–CuS	9 nm sized NPs were tested for their multimodal imaging *in vitro*/*in vivo* using a SKOV3 (human adenocarcinoma cell line)/tumor model	Simultaneous MRI, PA and PTT possible and *in vivo* studies on a SKOV3 tumor model showed excellent anticancer effects. However, long-term toxicity data needed	151

Table 3 (*Contd.*)

Specific application	Materials	Highlights	Remarks	Ref.
PTT/PDT	Ce6-modified carbon dots	Mean hydrodynamic diameters of RCDs and Ce6-RCDs are found to be around 9.8 and 9.9 nm, respectively	Multimodal-imaging-guided and single-NIR-laser-triggered photothermal/photodynamic synergistic cancer therapy on mouse mammary gland cancer cell line, 4T1 model	152
PDT	Biodegradable hollow $MoSe_2$/Fe_3O_4 anospheres	The particle size (400–150 nm) and the shell thickness (40–20 nm) were further adjusted by the addition of F-127	PDT-enhanced agent for multimode CT/MR/IR imaging and synergistic antitumor therapy on an H22, mouse liver tumor bearing model	153
PTT	Clearable black phosphorus nanoconjugate	~7 nm particle size	For targeted cancer phototheranostics on a mouse mammary gland cancer cell line, 4T1 model	154
PTT	Coated carbon nanospheres with patchy gold	For production of highly efficient photothermal agent	Improved therapeutic benefits on a human breast tumor model (MCF7)	155
PTT	Mn-porphyrin metal–organic frameworks	The size of NMOFs was 60 × 140 nm (TEM)	MRI-guided nitric oxide and PTT synergistic therapy on a human breast tumor (MCF7) model	156
PTT	PB@Au core–satellite multifunctional nanotheranostics	CSNPs have 138.8 nm particle size and −10 mV zeta potential	MR/CT imaging, *in vivo* and synergetic photothermal and radiosensitive therapy have been confirmed on a mouse mammary gland cancer cell line, 4T1 tumor model	157
PTT	Gd/CuS-loaded functional nanogels	These composite NPs are 85 nm sized and have specific targeting capability for FA over-expressing cancer cells	MRI/PAI-guided tumor-targeted PTT has been tested on human papilloma cancer cell line, KB bearing BALB/c mice.	158
PTT	Carbon dots/Prussian blue satellite/core nanocomposites	50 nm as overall size	The therapeutic effects were tested on a rat brain cancer cell line, C6 glioma bearing mouse model	159
PTT	Development of multifunctional clay-based nanomedicine	For elimination of primary invasive breast cancer and prevention of its lung metastasis and distant inoculation	The multifunctional clay medicine was studied on a mouse mammary gland cancer cell line, 4T1 bearing tumor model	160
PTT	Noncovalent ruthenium(II) complexes–single-walled carbon nanotube composites infrared irradiation	The lengths of the Ru@SWCNTs ranged from 20 nm to several micrometers	Bimodal photothermal and photodynamic therapy tested on a human epitheloid cervix cancer cell line, HeLa tumor bearing mouse model	161

was confirmed by MRI. The temperature rise was higher in the magnetically targeted group than in the non-targeted group (~12 °C *vs.* 8.5 °C). Systemically injected NPs showed maximum efficacy analysis with this simultaneous photo-magnetic treatment strategy under external NIR irradiation.[140]

Similarly, black phosphorus (BP) is a 2D layer-structured nanomaterial, where those independent layers are stacked by weak van der Waals forces almost similar to those of pristine graphite. BP-based NPs are considered to be a promising bio–inorganic nanomaterial.[141] Ren *et al.* made a multi-potent therapeutic system comprising amino-modified, porous silica nanohybrids (FMSNs). The as-made nanohybrids had a large surface area and pore volume, enhancing the attachment of DOX, and BP QDs (PTT agent). In addition, this could induce an improved PTT and bio-stability of degradable BP-QDs.[100] *In vitro*/*in vivo* studies clearly demonstrate that these BP-based inorganic nanohybrids have superior anti-cancer activities compared to single chemo and PTT.

For example, Ramasamy *et al.* developed $mSiO_2$-capped Au nanorods covered with nano-selenium overcoat (Se–Au/$mSiO_2$/DOX) nanohybrids. These multi-potent nanohybrids were developed to impart collective actions such as therapy and chemo-prevention, along with hyperthermic photo-ablation to cancer cells, expecting enhanced therapeutic benefits against multi-drug-resistant breast cancers (Fig. 6A).[93] The *in vivo* study confirmed effective accumulation in the tumor and the intra-tumoral release could be well controlled by external NIR laser irradiation (Fig. 6B). The *in vivo* therapeutic mechanistic

analysis showed that tumor inhibition was mainly through cell cycle arrest by Src/FAK/AKT pathways. The excellent synergy through an Se PTT/chemo combined effect enabled excellent anti-tumor effects by delaying tumor progression in *in vivo* studies (Fig. 6C and D).[93] The pre-clinical studies clearly showed that these novel inorganic nanohybrids are clinically relevant for further studies for translational applications.

WS_2-nanosheets were used with an iron oxide NP (IONP) coating on their surface, and further functionalized with $mSiO_2$ followed by PEG stabilization to make WS_2–IO@MS–PEG biohybrids. These nanohybrids were effective agents for multimodal imaging and therapy, specifically PTT.[100] Chemo-drug DOX loaded in the $mSiO_2$ shell in the nanohybrid could be released depending on external NIR exposure for effective PTT towards cancer cells. The *in vitro* results were further validated with *in vivo* experiments confirming their effectiveness for multimodal image-guided cancer therapy in combination with chemo and PTT.

Jin *et al.* developed a brand new theranostic platform based on Co–P nanohybrids as the core, shelled with $mSiO_2$ which was further decorated with MnO_2 as a pH-sensitive bi-modal MRI guided chemo/photo thermal agent in *in vitro*/*in vivo* applications (Fig. 7A). The core Co–P could be well utilized for an effective MRI-guided PTT, thanks to their NIR sensitivity and magnetic characteristics which allowed them to be used as bimodal imaging agents. The gatekeeper MnO_2, being acid labile, could dissolve into Mn^{2+} ions in addition to their T1-contrasting properties. This kind of multi-potent theranostic system would be able to give better detailed contrast information about the pathogenic tissue in pre-clinical evaluation using animal models (Fig. 7B–F). The pre-clinical evaluation of these inorganic–inorganic nanohybrids clearly confirmed their potential as an effective multimodal imaging-guided PTT agent to treat cancers. We hope that such nanohybrids would also be useful for treating deep-rooted cancers where better penetration of PTT agents is necessary.[142]

Advanced pancreatic cancer patients can be treated with imaging-guided interventional therapy since it is an effective and invasive and targeted drug-delivery system. The effectiveness of such a treatment regimen relies on high-resolution imaging and complete removal of cancer cells, specifically in the peripheral region along with a distant metastasized area, to make sure that there will be no recurrence on-going. To impart such advantages, hollow $mSiO_2$ NPs, Gem-PFH-Au-star-HMS-IGF1, were developed. Here, gemcitabine (Gem) and perfluorohexane (PFH) were loaded in the core, while Au nanostars (NSs) and insulin-like growth factor-1 (IGF1) were functionalized on the surface of the nanohybrids. This hybrid construct enhanced multimodal ultrasound (US)/CT/PAI/thermal imaging-guided PTT, with real-time monitoring. A thermo-responsive gel that solidifies at body temperature was used to enhance Gem release control and with single-administration, the patient-derived xenograft (PDX) mouse model was effectively treated by this therapy. Cell death of the remaining viable pancreatic cancer cells was achieved by Gem, eliminating further chances of recurrence.[143]

Another inorganic–inorganic nanohybrid was reported based on Se–SiO_2–FA–CuS/DOX which can be well localized in tumor tissues, inducing effective PTT on NIR exposure along with chemotherapy *via* DOX and Se release. Since the synergistic effect is due to the combined release of DOX and Se *via* chemotherapy and PTT, these nanohybrids are expected to have excellent *in vitro* effects on cancer cells which might be translated into *in vivo* conditions as well. Such nanohybrids could effectively terminate tumors due to their dual function *via* chemo and PTT. The well-known, unwanted side-effects of DOX in *in vivo* conditions might be reduced significantly because of Se, an added advantage for this theranostic system. All these properties make this inorganic–inorganic nanohybrid system a suitable chemo-photo-thermal ablating agent with no serious side-effects for future clinical applications.[144]

Au nanostar modified, perfluorohexane (PFH)-loaded hollow $mSiO_2$ nanocapsules (HMS) were further PEGylated for multimodal (US/CT/PAI)/thermal imaging, along with PTT. HMSs were silanized to obtain thiol surface groups, and coated with Au NPs *via* an Au–S bond. Au NS modified HMSs were further loaded with PFH inside the HMSs followed by thiolated PEGylation on the surface to make multifunctional HMSs@Au–PFH–mPEG NSs (HAPP for short) (Fig. 8A). Multimodal HAPP showed significant therapeutic benefit on a C6 tumor model with US/CT/PAI/thermal imaging after intravenous or intratumoral injection.[145]

Multifunctional dual-modal PEG-coated iron-doped copper sulfide (Cu_5FeS_4-PEG) NPs were developed for tumor imaging/PTT applications. The obtained Cu_5FeS_4-PEG NPs with high NIR absorbance could be used for PA imaging and PTT, while Fe^{3+} doping offers the NPs an additional property for MRI. Intravenously administered Cu_5FeS_4-PEG had significantly higher tumor uptake ($\sim$10% ID g^{-1}) as per PAI. These NPs showed significant therapeutic benefits on a 4T1 bearing mouse model.[146]

In another study, 2D reduced graphene oxide supported an Au nanostar (rGO/AuNS) nanocomposite made by the seed-mediated growth method (Fig. 8B) for synergistically killing multidrug-resistant bacteria. The prickly/sharp-edged nanostructure of these composite NPs enhanced their prominent antibacterial property by damaging the cell walls/membranes. The cell viability was 32% for methicillin-resistant *Staphylococcus aureus* (MRSA) when incubated with these NPs. When exposed to an 808 nm NIR laser, complete bacterial death was achieved through the PTT effects of rGO/AuNS.[147] NaBiF4:Gd-PDA-PEG NPs have been developed by integrating T1-MRI (MRTI) for precisely tracking photothermal agents with real-time MRI guidance (T1) for *in vivo* thermal variations during PTT (Fig. 8C). The extremely weak susceptibility (1.04×10^{-6} emu g^{-1} Oe^{-1}) of the developed nanohybrid, due to marginal interaction with the local phase, allowed the precise recording of real-time thermal variations in intra- and peri-tumoral healthy *vs.* tumoral tissues in MRI. 19 s per frame was the time resolution with a precision detection of $\sim$0.1 K for the thermal changes. This approach helps to achieve MRI/guided PTT for a wide variety of relevant clinical applications.[150] Biocompatible PTT agents are of greatest interest as they can

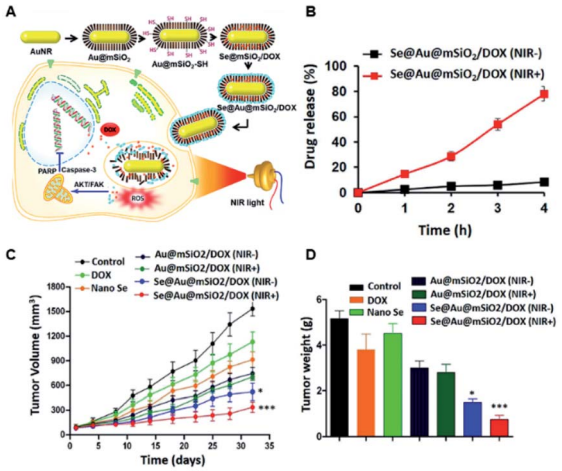

Fig. 6 (A) Schematic illustration for selenium–Au@mSiO$_2$/DOX (Se@Au@mSiO$_2$/DOX) for NIR-sensitive chemo-PTT. (B) *In vitro* DOX-release profile from the hybrid NPs with and without NIR exposure (808 nm, 2 W cm^{-2} for 5 min); *in vivo* therapeutic efficacy of the nanohybrids confirmed by (C) tumor volume changes and (D) non-toxic post-treatment effects (in terms of their body weight changes) observed in female BALB/c athymic nude mice bearing MDA-MB-231 xenografts after treatment with different formulations. The formulations were administered *via* the tail vein at a fixed dose of 5 mg kg^{-1} as DOX on days 1, 4, and 7. Data are presented as the mean ± SE ($n = 7$). *$p < 0.01$ and ***$p < 0.001$ compared to a control.[93] Reproduced from ref. 93 with permission from Nature Publishing Group, copyright 2018.

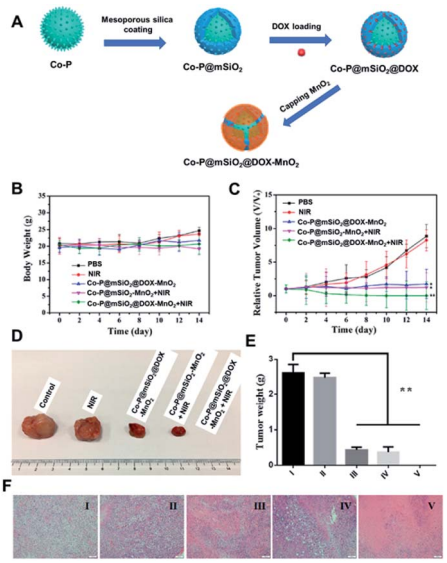

Fig. 7 (A) Illustration for the synthesis steps involved in Co–P–mSiO$_2$–DOX–MnO$_2$. (B) Body weight analysis post-treatment; (C) tumor volume changes post-treatment. (D) Images for the corresponding tumors after euthanasia post-treatment. (E) Tumor weights and (F) representative tumor histology images for various treated groups after treatments ((I) PBS solution as control; (II) NIR; (III) Co–P@mSiO$_2$@-DOX–MnO$_2$; (IV) Co–P@mSiO$_2$–MnO$_2$ + NIR; (V) Co–P@mSiO$_2$@-DOX–MnO$_2$ + NIR; *$p < 0.05$ and **$p < 0.01$ by the Student's two-tailed *t*-test).[142] Reproduced from ref. 142 with permission from the American Chemical Society, copyright 2017.

facilitate theranosis in a better way than conventional PTT agents. In order to achieve this, a Gd-modified CuS nano-theranostic agent (Gd:CuS@BSA) was prepared with a BSA bio-template (Fig. 8D). These 9 nm sized NPs showed high PTT efficiency with significant photo-stability under NIR laser irradiation. These NPs had excellent PA/MRI modalities with excellent hepatic clearance from the body. Therapeutic benefits have been studied in a SKOV3 tumor model (Fig. 9A–F).[151]

Au/carbon-based hybrid NPs are expected to possess combinatorial NIR light absorption and could have improved PTCE (photothermal conversion efficiency). To achieve this, a patchy gold coating on the carbon nanospheres *via* a facile adsorption–reduction method was adopted in order to give these composite NPs a Janus structure. The study clearly confirmed that these inorganic–inorganic nanohybrids have better PTCE as well as better thermal stability than traditional PTT agents, as was confirmed using various *in vitro* as well as *in vivo* experiments.[155]

MRI-guided nitric oxide and photothermal synergistic therapy was accomplished using an Mn-porphyrin MOF. Since nitric oxide (NO) therapy in combination with imaging-guided physical therapy is a promising alternative for clinical purposes, a nanoscale MOF (NMOF) integrating MRI, NO, and PTT was developed as a promising theranostic agent. The concept was proved by establishing NMOFs with Zr^{4+} ions and Mn-porphyrin as a bridging ligand. Introducing paramagnetic Mn ions into porphyrin rings allows us to achieve a significantly high T1-weighted MRI property and high PTCE. Thermal-induced NO generation was achieved by *S*-nitrosothiol (SNO) on the NMOF surfaces. Interestingly, single NIR light exposure simultaneously allowed NO as well as PTT. Intravenously injected NPs showed maximum therapeutic benefits, as confirmed using an *in vivo* MCF7 bearing tumor model.[156]

Multifunctional nano-theranostic PB@Au core–satellite NPs (CSNPs) were made by using Prussian blue NPs (PBNPs) and AuNPs. These integrated NPs have specific roles for MRI and CT imaging and synergistic PTT and radiotherapy (PTT–RT), as confirmed using 4T1 tumor bearing mice.[157]

Second NIR (NIR-II, 1000–1700 nm) therapy has recently attracted attention, especially in cancer management, mainly due to its two major properties: (1) low scattering ability and (2) deep penetration capability compared to the NIR-I (700–950 nm) region. NIR-II light absorbing NPs have been made of a Gd and CuS based nanogel (NG) platform for MRI/PAI dual imaging-guided tumor-targeted photo-therapy. Cross-linked PEI NGs were modified with Gd chelates, FA through a PEG spacer and 1,3-propanesultone. Finally, CuS NPs were loaded into these modified NGs. These aqueous dispersible 85 nm sized NGs have a very good protein resistance character with good reflexivity (11.66 mM^{-1} s^{-1}), along with a high NIR-II absorption capability. In addition, they have an excellent PTCE of ~26.7%. These nanohybrids were well homed into the tumor *via* an FA targeting pathway, as confirmed by KB-bearing BALB/c mice.[158]

A simple and economic, ecofriendly technique was used to design and fabricate carbon dot (CD) modified Prussian blue (PB NPs) (CDs/PBNP) hybrids with a satellite/core structure. The

CDs/PBNPs possess distinct green PL emission and NIR photoabsorption with high efficiency and photothermal stability. These biocompatible composite NPs were tested on a C6 brain glioma bearing mouse tumor model, confirming that CDs/PBNPs possess promising imaging and effective tumor ablation properties.[159]

It is well known that the PTCE (η) of Au NRs can be well tuned with an enlarged aspect ratio, and preferably with a core–shell structure. Such a core–shell GNR-LDH nanostructure constructed with GNRs and LDHs has been developed. The Au and LDH interaction allows an electron deficiency on the Au surface, inducing thermal energy conversion. When exposed to an 808 nm laser, these GNR@LDH had ~60% η, and dramatically improved PTCE over already-existing GNR-based PTT agents. These core–shell inorganic–inorganic composite NPs can be applied in various biomedical fields, such as PTT, as antibacterials, and in cancer therapy and bio-imaging with lower dose and nontoxicity.[162]

There is an NIR light-regulated bio-sensing technique which utilizes Pt@Au nanoring@DNA (PAD) probes for fluorescence-guided PTT on tumor cells. The developed nanohybrids have an Au nanoring and Pt framework (Pt@AuNR) acting as a photosensitizer and functionally modified double-stranded DNA (dsDNA) hybrids as a sensor. Thermo-sensitive de-hybridization of dsDNA localized on the PAD probe allows specific cellular recognition and NIR fluorescence imaging guided PTT upon laser exposure.[163]

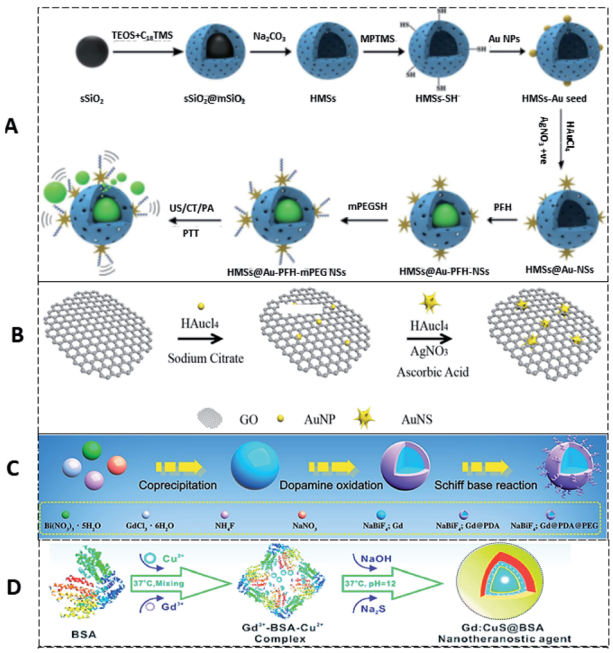

Fig. 8 (A) Schematic illustration of the synthesis of HMSs, HMSs@Au NSs, and HAPP,[145] reproduced from ref. 145 with permission from the American Chemical Society, copyright 2017. (B) rGO/Au NSs nanocomposite,[147] reproduced from ref. 147 with permission from the American Chemical Society, copyright 2019. (C) $NaBiF_4$:Gd-PDA-PEG NPs,[150] reproduced from ref. 150 with permission from the American Chemical Society, copyright 2020. (D) Gd:CuS@BSA NPs,[151] reproduced from ref. 151 with permission from the American Chemical Society, copyright 2016.

5.2 Inorganic–inorganic nanohybrids for combined PDT/imaging applications

Up-conversion materials (UC) have been widely used for PDT applications, mainly because they can solve the limitations associated with low tissue penetration, and overheating by excited 980 nm NIR light, and an insufficient amount of photosensitizing agents.

$NaGdF_4$:Yb/Tm@$NaGdF_4$:Yb@$NaNdF_4$:Yb@$NaGdF_4$@-$mSiO_2$@TiO_2 (UCNPs@$mSiO_2$@TiO_2) nanohybrids were successfully developed through TiO_2 PSs/photocatalyst coating on an effective 808 nm-to-UV/visible up-conversion luminescent (UCL) core. This nanohybrid system could be used for multimodal imaging along with PDT. *In vivo* studies on H22 (murine hepatocarcinoma) as the xenograft mode clearly showed that these NPs are non-toxic multimodal/PDT agents, making them suitable for further clinical trials.[164]

A similar study was conducted by Wu *et al.* (2020), where the research group developed an NIR light responsive UC material for effective PDT along with imaging capability. The nanohybrid system was based on $mSiO_2$-coated $NaGdF_4$:Yb,Er@$NaGdF_4$:-Yb,Nd. Even though the *in vitro* results are promising, the lack of pre-clinical studies using an animal model makes it difficult to predict their clinical relevance.[165]

5.3 Inorganic–inorganic nanohybrids for combined PTT/PDT/imaging applications

BSA-stabilized Gd_2O_3–Au nano crystals (NCs) were made as contrast agents in MRI and CT imaging (Fig. 10). AuNCs show fluorescence as well PDT properties by producing singlet oxygen under NIR at 808 nm. Coating BSA on these NPs served as

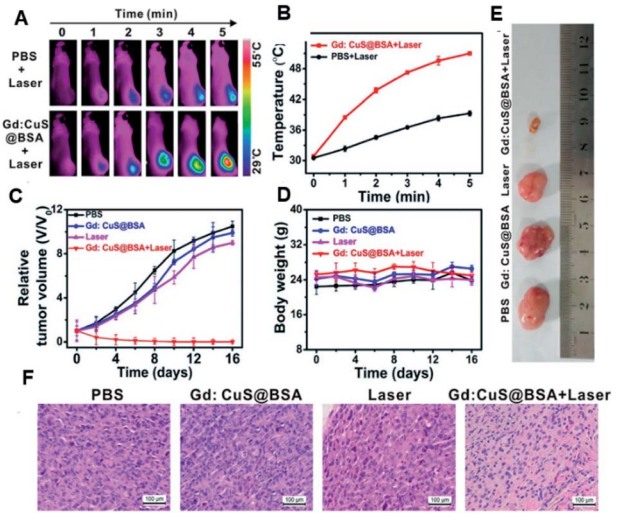

Fig. 9 *In vivo* PTT effects. (A) Thermal imaging of SKOV-3 tumor-bearing mice pre- and post-injection with PBS or nanohybrids under 980 nm laser exposure for 5 min. (B) Corresponding intra-tumoral PTT temperature changes; (C) relative tumor volume changes; (D) body weight analysis during the therapy. (E) Representative excised tumor images after euthanizing the animals and (F) corresponding histology analysis for each group, as shown in (E).[151] Reproduced from ref. 151 with permission from the American Chemical Society, copyright 2017.

a carrier for an ICG (Indo Cyanine Green) PTT agent. Thus, the composite NPs showed multifunctional properties, such as imaging and combined PTT/PDT. The imaging capabilities were tested using *in vivo* Kunming mice without any studies on the therapeutic benefits.[148]

Chlorin e6 (Ce6) and hyaluronic acid (HA) were composited with ultra-small MoS_2/nanodot biodegradable SiO_2 NPs for clearable multi-imaging-guided simultaneous PTT/PDT phototherapy. A 4T1 bearing tumor model was used for understanding its therapeutic as well as imaging benefits and the studies proved the major points that the authors had claimed (Fig. 11).[149]

The drawbacks associated with multimodal dual PTT/PDT therapy include the need for exposure to a high-power laser which has limited benefit due to intra-tumoral hypoxia. Additionally, two excitation laser sources are required to separately activate the PTT/PDT technique. Besides that, high-power laser irradiation for PTT is required and this problem has not been resolved. To solve these issues, a single-laser PTT/PDT triggerable technique with a smaller amount of photo-sensitizer loaded with PTT agent was reported by Sun *et al.* To confirm this idea, a small quantity of photo-sensitizer chlorin e6 (Ce6) (0.56% by mass) was functionalized onto amino-rich red-emissive carbon dots (RCDs) with significantly higher PTT effects under 671 nm NIR laser exposure. Interestingly, the same laser can be used to activate PDT *via* Ce6. These novel inorganic-nanohybrids were very promising as they could impart multiple functions under a single roof where one could make use of PTT and PDT along with bi-modal imaging such as photo-acoustic and fluorescence based imaging.[152]

Wen *et al.* developed FA-modified MT-LPTX–FA nanohybrids. This was based on the *in situ* formation of tellurium nanodots (Te NDs) in PTX-loaded LDH modified with $mSiO_2$ NPs.[89] The newly made nanohybrids showed excellent *in vitro* PDT and PTT actions along with intra-cellular pH-responsive drug release. Further, selective cancer targeting was achieved mainly due to the FA coating.

FA-targeted bio-non-accumulating black phosphorus nanoconjugates were made for cancer photo-theranostics (combined PTT/PDT). For this, copper sulfide nanodot anchored FA-modified black phosphorus nanosheets (BP–CuS–FA) were made which had better therapeutic efficiency of PDT–PTT when conjugated with FA. *In vivo* tracking was possible *via* the PAI properties of the developed NPs. A highlight is that these NPs can undergo renal clearance once they enter the body after PTT/PDT. The therapeutic effects were studied on a 4T1 tumor model.[154]

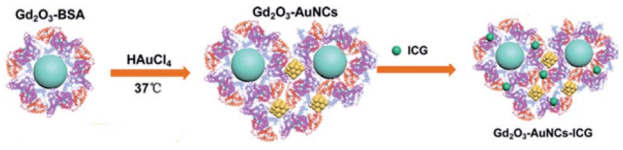

Fig. 10 Preparation of Gd_2O_3–AuNC nanohybrid.[148] Reproduced from ref. 148 with permission from the American Chemical Society, copyright 2017.

Ru(II) complex-modified single-walled carbon nanotubes (Ru@SWCNTs) were developed as nanotemplates for bimodal PTT and two-photon PDT. The π–π interactions allowed SWCNTs to interact and load a significantly high amount of Ru(II) complexes (Ru1 or Ru2). On NIR exposure (808 nm diode laser (0.25 W cm^{-2})), TPDT is achieved through the Ru(II) complexes by generating singlet oxygen. Taking advantage of both PTT and two-photon PDT, these novel nanohybrids showed better therapeutic outcomes compared to their individual therapies. The bi-modal therapeutic efficacy was confirmed using a tumor model. *In vivo* tumor (HeLa tumor model) ablation was achieved with excellent treatment efficacy under 808 nm irradiation at a power density of 0.25 W cm^{-2} for 5 min. Preliminary analysis clearly showed that this bimodal therapeutic approach would be beneficial for treating various cancers.[161]

Similarly, a tri-modal imaging-guided inorganic PDT/PTT nanohybrid was developed in order to achieve CT/MRI/IR imaging plus PDT/PTT for antitumor therapy. The nanohybrid was based on $MoSe_2/Fe_3O_4$ nanospheres, whose size and hollow topography can be tuned by F-127 modification. Compared to pristine $MoSe_2$, the modified nanohybrid $MoSe_2/Fe_3O_4$ doubled the generation of reactive oxygen species (ROS), with twofold ROS generation helping to achieve PDT.[153] Since most of the deep-rooted tumors are suffering hypoxia conditions, the newly developed nanohybrids are expected to overcome such biological barriers. In order to achieve better penetration in such circumstances, it is essential to load perfluorocarbon (PFC) and O_2 onto nanohybrids of hollow $MoSe_2/Fe_3O_4$ (MF-2) to make O_2@PFC@MF-2, which is expected to triple ROS production. The as-made nano–bio hybrids have a narrow band gap and a hollow structure which help to achieve higher PTCE. Fe_3O_4 in the nanohybrids is expected to improve the biodegradation by accelerating an endogenous redox reaction to form aqueous soluble Mo-VI-oxide species. The model drug, DOX attached onto the nanohybrids would impart chemo-effects as well. In

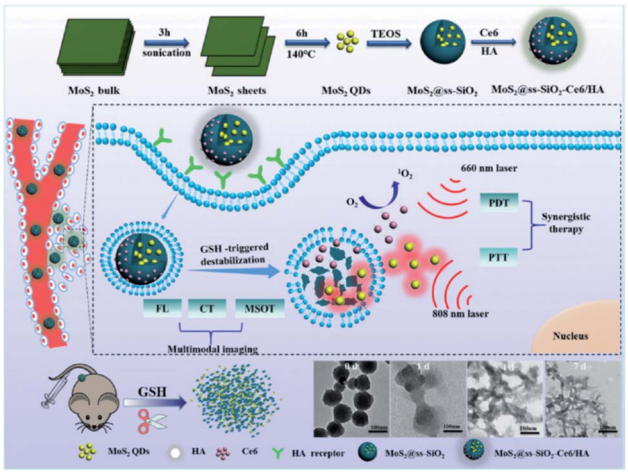

Fig. 11 Synthesis and mechanism of MoS_2@ss-SiO_2-Ce6/HA nanocomposites and subsequent GSH-triggered biodegradable phenomenon and renal clearance.[149] Reproduced from ref. 149 with permission from the American Chemical Society, copyright 2017.

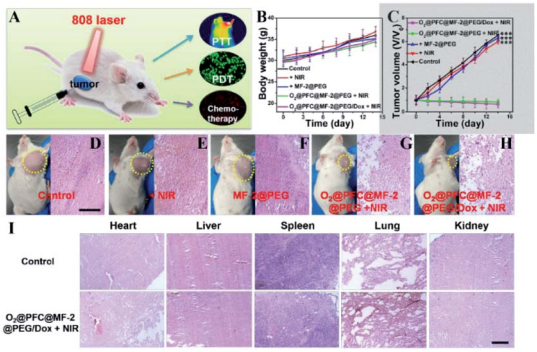

Fig. 12 *In vivo* evaluation: (A) scheme represents the treatment method. Body weight changes (B) and relative tumor volume (C) achieved after various treatments. (D–H) Photographs of mice and H&E stained images of tumor tissues obtained after two weeks of treatment. (I) H&E stained images of heart, liver, spleen, lung and kidney obtained from various groups after two weeks of treatment (scale bars: 15 μm, ***$p < 0.001$).[153] Reproduced from ref. 153 with permission from the American Chemical Society, copyright 2019.

a nutshell, these inorganic nanohybrids are best for multi-functional image-guided PTT/PDT/chemo-therapy (Fig. 12A–I).[153] Similarly, biodegradable, immuno carbon/silica nano-hybrids showed excellent PTT/PDT *in vivo* using a 4T1 tumor model as well as a patient-derived xenograft model.[166]

6. Conclusions and future perspectives

In the current review, we have focused mainly on inorganic–inorganic nanohybrids that have been explored for various biomedical applications, as highlighted. Apart from the very few commercially available inorganic nanohybrids for practical medical applications, there are so many such nanohybrid systems that only end up as just "publications". One has to really think about it and work on bringing such pipeline work into commercial applications in terms of real-life usage. The major difficulty in bringing such kinds of work to reality is associated with toxicity issues. Of course, there have been tremendous efforts in making new functional inorganic–inorganic nanohybrids along with *in vivo* imaging applications.[167] Here one of the major problems noted is that most such work has not given any deserved attention to the toxicity area, limiting its clinical applicability. For example, a recent study used iron–gold (Fe–Au) composite nanohybrids as potential exogenous contrast agents for Magnetomotive Optical Coherence Tomography using an animal model. This study did not give any information about adverse effects on the animal they had used.[168] On the other hand, there are studies highlighting the negative impacts of nanohybrid materials as well. Chen *et al.* (2020) studied the toxicity on the eye of mesoporous silica/Ag nanohybrids using a rat animal model, showing that even a safe dosage could cause adverse effects such as dry eye and corneal damage. They advised that these negative impacts could be reduced by fetal bovine serum (FBS) treatment.[169]

Even so, we have few commercially available T1 contrasting agents, which are not under the category of inorganic–inorganic nanohybrids. In fact, they are inorganic–organic nanohybrids. Magnevist (Gd-DTPA) and Dotarem (Gd-DOTA) are a couple of examples of T1 contrast agents.[170,171] Unfortunately, Gd–chelator complexes have been reported to have serious limitations mainly associated with Gd^{3+} ion leaching, which can accumulate in the body. Since they are unable to be metabolized, clearance would be difficult, leading to severe detrimental effects to humans, including nephrogenic system fibrosis in patients with renal dysfunction, and may also inhibit calcium channels.[172] In some recent reports, engineered Gd^{3+} ions with nanocarriers have been proved to be effective in preventing leaching while enhancing T1-shortening capacity. Nevertheless, looking at the number of publications in this relevant area is actually giving us hope that there are aggressive ongoing studies either to improve or to modify the existing strategies.

However, since we are concerned about clinical applications, exclusive attention should be given to the area where their actual application should be tested vigorously using pre-clinical tests on animal models. Typically, in *in vivo* clearance of hybrid nanosystems, their safety effects on major organs, such as the heart, kidney, liver, brain, stomach, spleen, and lungs, should be tested in detail using various pharmaco-kinetic and pharmaco-dynamic studies, including bio-distribution clearance, organ accumulation and histo-pathology evaluation. Specifically, long-term exposure to such inorganic nanohybrids should be evaluated in the same way to make sure that the newly developed inorganic–inorganic nanohybrid materials are safe for clinical translations.

It is also very important to choose proper materials for making novel nanohybrid materials. The LDH-based hybrid NP

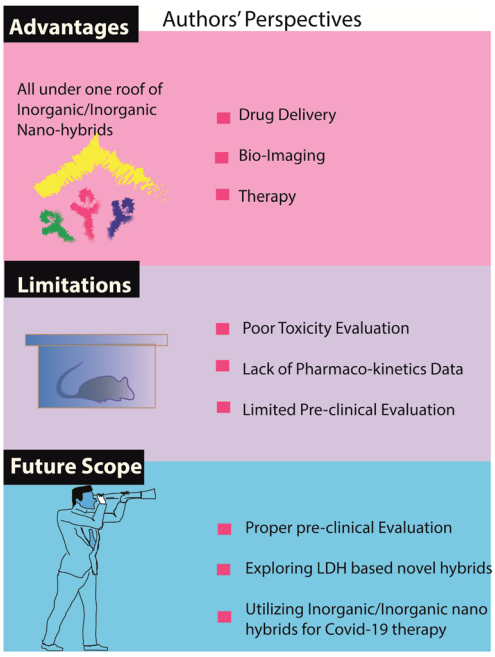

Scheme 2 Authors' perspectives on the advantages, limitations and future scope of emerging inorganic–inorganic nanohybrids.

research area should be well utilized for making novel inorganic–inorganic nanohybrids, mainly because they are biodegradable and biocompatible in nature. Recent developments in LDH-based nanohybrid materials clearly show that next-generation nanohybrid materials are most likely to be LDH based. In addition, LDH's acidically degradation could lead to the development of various pH-sensitive nanohybrids specifically for anti-tumor applications, where one can modify their surface to boost selective targeting to cancers without harming normal/healthy cells. Additionally, during the ongoing pandemic situation, inorganic chemists can think of utilizing these novel inorganic based hybrids for treating the SARS-Cov-2 virus as well. The authors' perspectives are summarized in Scheme 2.

Yes, there is still hope that inorganic–inorganic nanohybrids could be beneficial since they are not just bare molecules as they used to be, but are hybridized with a suitable biocompatible counterpart. Therefore, such newly made bio-functional nanohybrids could reduce all the negative aspects of their single entities, leading to them having novel properties, making them stable, human-friendly biomaterials for various biomedical applications, including drug delivery, bio-imaging and photothermal/dynamic therapy.

Conflicts of interest

There are no conflicts to declare.

Acknowledgements

This research was supported by Basic Science Research Program through the National Research Foundation of Korea (NRF) funded by the Ministry of Education (No. 2020R1I1A2074844), by the NRF grant funded by the Korea government (MSIT) (No. 2020R1F1A1075509), and under the framework of the International Cooperation Program managed by NRF (2017K2A9A2A10013104).

Notes and references

1 X. Y. Zhang, *Eur. Rev. Med. Pharmacol. Sci.*, 2015, **19**, 220–224.
2 D. Chen, C. A. Dougherty, K. Zhu and H. Hong, *J. Controlled Release*, 2015, **210**, 230–245.
3 A. Fernandez-Fernandez, R. Manchanda and A. J. McGoron, *Appl. Biochem. Biotechnol.*, 2011, **165**, 1628–1651.
4 G. Sai-Anand, A. Sivanesan, M. R. Benzigar, G. Singh, A.-I. Gopalan, A. V. Baskar, H. Ilbeygi, K. Ramadass, V. Kambala and A. Vinu, *Bull. Chem. Soc. Jpn.*, 2018, **92**, 216–244.
5 B. L. Li, M. I. Setyawati, L. Chen, J. Xie, K. Ariga, C.-T. Lim, S. Garaj and D. T. Leong, *ACS Appl. Mater. Interfaces*, 2017, **9**, 15286–15296.
6 K. Ariga, T. Mori and J. Li, *Langmuir*, 2019, **35**, 3585–3599.
7 K. Ariga, *Langmuir*, 2020, **36**, 7158–7180.
8 S. Eom, G. Choi, H. Nakamura and J.-H. Choy, *Bull. Chem. Soc. Jpn.*, 2019, **93**, 1–12.
9 R. van der Meel, E. Sulheim, Y. Shi, F. Kiessling, W. J. M. Mulder and T. Lammers, *Nat. Nanotechnol.*, 2019, **14**, 1007–1017.
10 S. Mukherjee, V. S. Madamsetty, D. Bhattacharya, S. Roy Chowdhury, M. K. Paul and A. Mukherjee, *Adv. Funct. Mater.*, 2020, **30**, 2003054.
11 J. H. Choy, S. J. Hwang and N. G. Park, *J. Am. Chem. Soc.*, 1997, **119**, 1624–1633.
12 J. H. Choy, J. H. Park and J. B. Yoon, *J. Phys. Chem. B*, 1998, **102**, 5991–5995.
13 J. H. Choy, H. Jung, Y. S. Han, J. B. Yoon, Y.-G. Shul and H.-J. Kim, *Chem. Mater.*, 2002, **14**, 3823–3828.
14 S. R. Lee, Y. S. Han, M. Park, G. S. Park and J.-H. Choy, *Chem. Mater.*, 2003, **15**, 4841–4845.
15 S. R. Lee, M. Park, Y. S. Han, S. H. Hwang and J. H. Choy, *J. Phys. Chem. B*, 2005, **109**, 9432–9436.
16 J. H. Park, J. H. Yang, J. B. Yoon, S. J. Hwang and J. H. Choy, *J. Phys. Chem. B*, 2006, **110**, 1592–1598.
17 J. H. Choy, S. J. Kwon and G. S. Park, *Science*, 1998, **280**, 1589–1592.
18 J. H. Choy, S.-J. Kwon, S. J. Hwang, Y. I. Kim and W. Lee, *J. Mater. Chem.*, 1999, **9**, 129–135.
19 J. H. Choy, Y. I. Kim, B. W. Kim, N. G. Park, G. Campet and J.-C. Grenier, *Chem. Mater.*, 2000, **12**, 2950–2956.
20 Y. S. Han, I. Park and J.-H. Choy, *J. Mater. Chem.*, 2001, **11**, 1277–1282.
21 S. J. Kwon, J.-H. Choy, D. Jung and P. V. Huong, *Phys. Rev. B: Condens. Matter Mater. Phys.*, 2002, **66**, 224510.
22 J. H. Choy, S.-Y. Kwak, J. S. Park, Y. J. Jeong and J. Portier, *J. Am. Chem. Soc.*, 1999, **121**, 1399–1400.
23 J. H. Choy, J. M. Oh, M. Park, K. M. Sohn and J. W. Kim, *Adv. Mater.*, 2004, **16**, 1181–1184.
24 T. S. Santra, C. H. Liu, T. K. Bhattacharyya, P. Patel and T. K. Barik, *J. Appl. Phys.*, 2010, **107**, 124320.
25 D. K. Lee, Y. S. Kang, C. S. Lee and P. Stroeve, *J. Phys. Chem. B*, 2002, **106**, 7267–7271.
26 L. Wang, Y. Ebina, K. Takada and T. Sasaki, *J. Phys. Chem. B*, 2004, **108**, 4283–4288.
27 E. Manias, A. Touny, L. Wu, K. Strawhecker, B. Lu and T. C. Chung, *Chem. Mater.*, 2001, **13**, 3516–3523.
28 J. H. Choy, S. M. Paek, J. M. Oh and E. S. Jang, *Curr. Appl. Phys.*, 2002, **2**, 489–495.
29 E. Katz and I. Willner, *Angew. Chem., Int. Ed.*, 2004, **43**, 6042–6108.
30 S. Förster and T. Plantenberg, *Angew. Chem., Int. Ed.*, 2002, **41**, 688–714.
31 A. Stein, B. J. Melde and R. C. Schroden, *Adv. Mater.*, 2000, **12**, 1403–1419.
32 J. H. Choy, H. C. Lee, H. Jung and S. J. Hwang, *J. Mater. Chem.*, 2001, **11**, 2232–2234.
33 A. Zanoletti, I. Vassura, E. Venturini, M. Monai, T. Montini, S. Federici, A. Zacco, L. Treccani and E. Bontempi, *Front. Chem.*, 2018, **6**, 60.
34 N. Zhao, L. Yan, X. Zhao, X. Chen, A. Li, D. Zheng, X. Zhou, X. Dai and F.-J. Xu, *Chem. Rev.*, 2019, **119**, 1666–1762.
35 S. Sreejith, T. T. M. Huong, P. Borah and Y. Zhao, *Sci. Bull.*, 2015, **60**, 665–678.

36 K. Katagiri, in *Bioceramics*, ed. A. Osaka and R. Narayan, Elsevier, 2021, pp. 113–135, DOI: 10.1016/B978-0-08-102999-2.00006-5.
37 D. Ma, in *Noble Metal-Metal Oxide Hybrid Nanoparticles*, ed. S. Mohapatra, T. A. Nguyen and P. Nguyen-Tri, Woodhead Publishing, 2019, pp. 3–6, DOI: 10.1016/B978-0-12-814134-2.00001-2.
38 J. Hernandez-Montelongo, C. Fernandez-Fierro, N. Benito-Gomez, M. Romero-Saez, J. Parodi, E. R. Carmona and G. Recio-Sanchez, *Mater. Sci. Eng., C*, 2020, **116**, 111183.
39 M. Gharbavi, B. Johari, N. Mousazadeh, B. Rahimi, M. P. Leilan, S. S. Eslami and A. Sharafi, *Mol. Biol. Rep.*, 2020, **47**, 6517–6529.
40 A. Sanchez, K. Ovejero Paredes, J. Ruiz-Cabello, P. Martinez-Ruiz, J. M. Pingarron, R. Villalonga and M. Filice, *ACS Appl. Mater. Interfaces*, 2018, **10**, 31032–31043.
41 Y. Lv, P. Liu, H. Ding, Y. Wu, Y. Yan, H. Liu, X. Wang, F. Huang, Y. Zhao and Z. Tian, *ACS Appl. Mater. Interfaces*, 2015, **7**, 20640–20648.
42 J. Chen, X. Li, X. Wu, J. T. Pierce, N. Fahruddin, M. Wu and J. X. Zhao, *Langmuir*, 2014, **30**, 9514–9523.
43 S. K. Ujjain, P. Ahuja and R. K. Sharma, *J. Mater. Chem. B*, 2015, **3**, 7614–7622.
44 S. C. Mohapatra, H. K. Tiwari, M. Singla, B. Rathi, A. Sharma, K. Mahiya, M. Kumar, S. Sinha and S. S. Chauhan, *J. Biol. Inorg Chem.*, 2010, **15**, 373–385.
45 M. Vahdati and T. Tohidi Moghadam, *Sci. Rep.*, 2020, **10**, 510.
46 Y. Miao, Z. Zhang, Y. Gong, Q. Zhang and G. Yan, *Biosens. Bioelectron.*, 2014, **52**, 271–276.
47 V. Perumal, U. Hashim, S. C. B. Gopinath, R. Haarindraprasad, K. L. Foo, S. R. Balakrishnan and P. Poopalan, *Sci. Rep.*, 2015, **5**, 12231.
48 R. Xing, A. A. Bhirde, S. Wang, X. Sun, G. Liu, Y. Hou and X. Chen, *Nano Res.*, 2013, **6**, 1–9.
49 S.-Y. Kwak, Y.-J. Jeong, J.-S. Park and J.-H. Choy, *Solid State Ionics*, 2002, **151**, 229–234.
50 G. Ramalingam, K. V. Saravanan, T. K. Vizhi, M. Rajkumar and K. Baskar, *RSC Adv.*, 2018, **8**, 8516–8527.
51 W. C. Law, K. T. Yong, I. Roy, H. Ding, R. Hu, W. Zhao and P. N. Prasad, *Small*, 2009, **5**, 1302–1310.
52 K. K. Pohaku Mitchell, A. Liberman, A. C. Kummel and W. C. Trogler, *J. Am. Chem. Soc.*, 2012, **134**, 13997–14003.
53 Y. Liu, Y. Tang, Y. Tian, J. Wu, J. Sun, Z. Teng, S. Wang and G. Lu, *ACS Appl. Nano Mater.*, 2019, **2**, 1194–1201.
54 O. Geuli, N. Metoki, T. Zada, M. Reches, N. Eliaz and D. Mandler, *J. Mater. Chem. B*, 2017, **5**, 7819–7830.
55 N. Chawda, M. Basu, D. Majumdar, R. Poddar, S. K. Mahapatra and I. Banerjee, *ACS Omega*, 2019, **4**, 12470–12479.
56 M. Henriksen-Lacey, S. Carregal-Romero and L. M. Liz-Marzán, *Bioconjugate Chem.*, 2017, **28**, 212–221.
57 M. Wu, Q. Meng, Y. Chen, L. Zhang, M. Li, X. Cai, Y. Li, P. Yu, L. Zhang and J. Shi, *Adv. Mater.*, 2016, **28**, 1963–1969.
58 G.-J. Ding, Y.-J. Zhu, C. Qi, B.-Q. Lu, F. Chen and J. Wu, *J. Mater. Chem. B*, 2015, **3**, 1823–1830.
59 Y. K. Lee, K. J. Yu, Y. Kim, Y. Yoon, Z. Xie, E. Song, H. Luan, X. Feng, Y. Huang and J. A. Rogers, *ACS Appl. Mater. Interfaces*, 2017, **9**, 42633–42638.
60 C. Tao and Y. Zhu, *Dalton Trans.*, 2014, **43**, 15482–15490.
61 J. Florek, R. Caillard and F. Kleitz, *Nanoscale*, 2017, **9**, 15252–15277.
62 A. Rahikkala, S. A. P. Pereira, P. Figueiredo, M. L. C. Passos, A. R. T. S. Araújo, M. L. M. F. S. Saraiva and H. A. Santos, *Adv. Biosyst.*, 2018, **2**, 1800020.
63 X. l. Tang, F. Jing, B.-l. Lin, S. Cui, R.-t. Yu, X.-d. Shen and T.-w. Wang, *ACS Appl. Mater. Interfaces*, 2018, **10**, 15001–15011.
64 C. Xu, M. Yu, O. Noonan, J. Zhang, H. Song, H. Zhang, C. Lei, Y. Niu, X. Huang, Y. Yang and C. Yu, *Small*, 2015, **11**, 5949–5955.
65 M. Bouchoucha, É. Béliveau, F. Kleitz, F. Calon and M.-A. Fortin, *J. Mater. Chem. B*, 2017, **5**, 7721–7735.
66 Y. Li, N. Li, W. Pan, Z. Yu, L. Yang and B. Tang, *ACS Appl. Mater. Interfaces*, 2017, **9**, 2123–2129.
67 H. Fan, X. Xing, Y. Yang, B. Li, C. Wang and D. Qiu, *Dalton Trans.*, 2017, **46**, 14831–14838.
68 L. Li, W. Gu, J. Liu, S. Yan and Z. P. Xu, *Nano Res.*, 2015, **8**, 682–694.
69 G. Choi, I.-R. Jeon, H. Piao and J.-H. Choy, *Adv. Funct. Mater.*, 2018, **28**, 1704470.
70 M. Kaur, P. Singh, K. Singh, U. S. Gaharwar, R. Meena, M. Kumar, F. Nakagawa, S. Wu, M. Suzuki, H. Nakamura and A. Kumar, *Mater. Lett.*, 2020, **259**, 126832.
71 G. Vares, V. Jallet, Y. Matsumoto, C. Rentier, K. Takayama, T. Sasaki, Y. Hayashi, H. Kumada and H. Sugawara, *Nanomedicine*, 2020, **27**, 102195.
72 X. Zhu, J. Han, H. Lan, Q. Lin, Y. Wang and X. Sun, *BMC Cancer*, 2020, **20**, 1190.
73 L. Zhou, Q. Xu, L. Huang, J. Jin, X. Zuo, Q. Zhang, L. Ye, S. Zhu, P. Zhan, J. Ren, T. Lv and Y. Song, *Cancer Lett.*, 2021, **500**, 163–171.
74 M. D. Tharmalingam, G. Matilionyte, W. H. B. Wallace, J. B. Stukenborg, K. Jahnukainen, E. Oliver, A. Goriely, S. Lane, J. Guo, B. Cairns, A. Jorgensen, C. M. Allen, F. Lopes, R. A. Anderson, N. Spears and R. T. Mitchell, *BMC Med.*, 2020, **18**, 374.
75 C. Chouaid, I. Monnet and N. Baize, *Lancet Oncol.*, 2020, **21**, e546.
76 S. H. Park, D. H. Lim, T. S. Sohn, J. Lee, D. Y. Zang, S. T. Kim, J. H. Kang, S. Y. Oh, I. G. Hwang, J. H. Ji, D. B. Shin, J. I. Yu, K. M. Kim, J. Y. An, M. G. Choi, J. H. Lee, S. Kim, J. Y. Hong, J. O. Park, Y. S. Park, H. Y. Lim, J. M. Bae and W. K. Kang, *Ann. Oncol.*, 2021, **32**, 368–374.
77 D. Tong, E. Zou, L. Bai, J. Ma, N. Guo, H. Wang and L. Jiang, *J. BUON*, 2020, **25**, 2205–2214.
78 P. F. Innominato, A. Karaboue, C. Focan, P. Chollet, S. Giacchetti, M. Bouchahda, A. Ulusakarya, A. Torsello, R. Adam, F. A. Levi and C. Garufi, *Int. J. Cancer*, 2020, DOI: 10.1002/ijc.33422.
79 K. Lin, Z.-Z. Zhao, H.-B. Bo, X.-J. Hao and J.-Q. Wang, *Front. Pharmacol.*, 2018, **9**, 1323.

80 C. H. Lin, S. H. Cheng, W. N. Liao, P. R. Wei, P. J. Sung, C. F. Weng and C. H. Lee, *Int. J. Pharm.*, 2012, **429**, 138–147.
81 C. Rejeeth, T. C. Nag and S. Kannan, *Cancer Nanotechnol.*, 2013, **4**, 127–136.
82 M. Kettering, H. Zorn, S. Bremer-Streck, H. Oehring, M. Zeisberger, C. Bergemann, R. Hergt, K. J. Halbhuber, W. A. Kaiser and I. Hilger, *Phys. Med. Biol.*, 2009, **54**, 5109–5121.
83 C. Xu, B. Wang and S. Sun, *J. Am. Chem. Soc.*, 2009, **131**, 4216–4217.
84 G. Lv, L. Qiu, G. Liu, W. Wang, K. Li, X. Zhao and J. Lin, *Dalton Trans.*, 2016, **45**, 18147–18155.
85 F. Muhammad, A. Wang, W. Qi, S. Zhang and G. Zhu, *ACS Appl. Mater. Interfaces*, 2014, **6**, 19424–19433.
86 Y. Liu, Y. Wu, R. Zhang, J. Lam, J. C. Ng, Z. P. Xu, L. Li and H. T. Ta, *ACS Appl. Bio Mater.*, 2019, **2**, 5930–5940.
87 E. P. Komarala, S. Nigam, M. Aslam and D. Bahadur, *New J. Chem.*, 2016, **40**, 423–433.
88 L. Li, Z. Gu, W. Gu, J. Liu and Z. P. Xu, *J. Colloid Interface Sci.*, 2016, **470**, 47–55.
89 J. Wen, K. Yang, X. Ding, H. Li, Y. Xu, F. Liu and S. Sun, *Inorg. Chem.*, 2019, **58**, 2987–2996.
90 E. Campbell, M. T. Hasan, C. Pho, K. Callaghan, G. R. Akkaraju and A. V. Naumov, *Sci. Rep.*, 2019, **9**, 416.
91 M. Ravichandran, S. Velumani, J. T. Ramirez, A. Vera and L. Leija, *Artif. Cells, Nanomed., Biotechnol.*, 2018, **46**, S993–s1003.
92 D. Diaz-Diestra, B. Thapa, D. Badillo-Diaz, J. Beltran-Huarac, G. Morell and B. R. Weiner, *Nanomaterials*, 2018, **8**, 484.
93 T. Ramasamy, H. B. Ruttala, P. Sundaramoorthy, B. K. Poudel, Y. S. Youn, S. K. Ku, H.-G. Choi, C. S. Yong and J. O. Kim, *NPG Asia Mater.*, 2018, **10**, 197–216.
94 L. Li, Z. Gu, W. Gu, J. Liu and Z. P. Xu, *J. Colloid Interface Sci.*, 2016, **470**, 47–55.
95 D. Diaz-Diestra, B. Thapa, D. Badillo-Diaz, J. Beltran-Huarac, G. Morell and B. R. Weiner, *Nanomaterials*, 2018, **8**, 484.
96 Y. Wang, X. Liu, G. Deng, J. Sun, H. Yuan, Q. Li, Q. Wang and J. Lu, *Nanoscale*, 2018, **10**, 2866–2875.
97 H. Qiao, Z. Cui, S. Yang, D. Ji, Y. Wang, Y. Yang, X. Han, Q. Fan, A. Qin, T. Wang, X.-P. He, W. Bu and T. Tang, *ACS Nano*, 2017, **11**, 7259–7273.
98 W. Cao, F. Muhammad, Y. Cheng, M. Zhou, Q. Wang, Z. Lou, Z. Li and H. Wei, *ACS Appl. Bio Mater.*, 2018, **1**, 928–935.
99 X. Ren, L. Shi, X. Yu, W. Liu, J. Sheng, J. Wan, Y. Li, Y. Wan, Z. Luo and X. Yang, *Nanoscale*, 2020, **12**, 12578–12588.
100 G. Yang, H. Gong, T. Liu, X. Sun, L. Cheng and Z. Liu, *Biomaterials*, 2015, **60**, 62–71.
101 R. Weissleder and M. J. Pittet, *Nature*, 2008, **452**, 580–589.
102 S. Dufort, L. Sancey, C. Wenk, V. Josserand and J. L. Coll, *Biochim. Biophys. Acta, Biomembr.*, 2010, **1798**, 2266–2273.
103 P. Padmanabhan, A. Kumar, S. Kumar, R. K. Chaudhary and B. Gulyás, *Acta Biomater.*, 2016, **41**, 1–16.
104 J. Key and J. F. Leary, *Int. J. Nanomed.*, 2014, **9**, 711–726.
105 J.-M. Oh, S.-J. Choi, S.-T. Kim and J.-H. Choy, *Bioconjugate Chem.*, 2006, **17**, 1411–1417.
106 S.-J. Choi, G. E. Choi, J.-M. Oh, Y.-J. Oh, M.-C. Park and J.-H. Choy, *J. Mater. Chem.*, 2010, **20**, 9463–9469.
107 P.-R. Wei, S.-H. Cheng, W.-N. Liao, K.-C. Kao, C.-F. Weng and C.-H. Lee, *J. Mater. Chem.*, 2012, **22**, 5503–5513.
108 J.-M. Oh, S.-J. Choi, G.-E. Lee, S.-H. Han and J.-H. Choy, *Adv. Funct. Mater.*, 2009, **19**, 1617–1624.
109 H.-E. Chung, D.-H. Park, J.-H. Choy and S.-J. Choi, *Appl. Clay Sci.*, 2012, **65–66**, 24–30.
110 S. J. Choi, J. M. Oh and J. H. Choy, *J. Ceram. Soc. Jpn.*, 2009, **117**, 543–549.
111 S. Das, S. Mukhopadhyay, S. Chatterjee, P. S. Devi and G. Suresh Kumar, *ACS Omega*, 2018, **3**, 7494–7507.
112 Y. M. Hao, S. Y. Lou, S. M. Zhou, R. J. Yuan, G. Y. Zhu and N. Li, *Nanoscale Res. Lett.*, 2012, **7**, 100.
113 S. Chinnathambi and N. Shirahata, *Sci. Technol. Adv. Mater.*, 2019, **20**, 337–355.
114 Q. Gu, F. Su, S. Ma, G. Sun and X. Yang, *Chem. Commun.*, 2015, **51**, 2514–2517.
115 Y. Xiang, X. F. Yu, D. F. He, Z. Sun, Z. Cao and Q. Q. Wang, *Adv. Funct. Mater.*, 2011, **21**, 4388–4396.
116 H. Chen and W.-G. Zhang, *J. Am. Ceram. Soc.*, 2010, **93**, 2305–2310.
117 Y. Chen, S. Zhou, F. Li and Y. Chen, *J. Mater. Sci.*, 2010, **45**, 6417–6423.
118 L. Liu, Q. Wang, C. Gao, H. Chen, W. Liu and Y. Tang, *J. Phys. Chem. C*, 2014, **118**, 14511–14520.
119 J.-M. Oh, T. T. Biswick and J.-H. Choy, *J. Mater. Chem.*, 2009, **19**, 2553–2563.
120 T.-H. Kim, J. Y. Lee, M.-K. Kim, J. H. Park and J.-M. Oh, *RSC Adv.*, 2016, **6**, 48415–48419.
121 S. Shi, B. C. Fliss, Z. Gu, Y. Zhu, H. Hong, H. F. Valdovinos, R. Hernandez, S. Goel, H. Luo, F. Chen, T. E. Barnhart, R. J. Nickles, Z. P. Xu and W. Cai, *Sci. Rep.*, 2015, **5**, 16930.
122 P. Puvanakrishnan, J. Park, P. Diagaradjane, J. A. Schwartz, C. L. Coleman, K. L. Gill-Sharp, K. L. Sang, J. D. Payne, S. Krishnan and J. W. Tunnell, *J. Biomed. Opt.*, 2009, **14**, 024044.
123 M. Z. Iqbal, X. Ma, T. Chen, L. e. Zhang, W. Ren, L. Xiang and A. Wu, *J. Mater. Chem. B*, 2015, **3**, 5172–5181.
124 W. Fang, W. Zhu, H. Chen, H. Zhang, S. Hong, W. Wei and T. Zhao, *ACS Appl. Bio Mater.*, 2020, **3**, 1690–1697.
125 H. Aoki, M. Nojiri, R. Mukai and S. Ito, *Nanoscale*, 2015, **7**, 337–343.
126 W. Li and X. Chen, *Nanomedicine*, 2015, **10**, 299–320.
127 V. Girardeau, O. Jacquin, O. Hugon, B. Riviere, B. van der Sanden and E. Lacot, *Appl. Opt.*, 2019, **58**, 7195–7204.
128 A. Walther, L. Rippe, L. V. Wang, S. Andersson-Engels and S. Kroll, *Biomed. Opt. Express*, 2017, **8**, 4523–4536.
129 S. Sreejith, J. Joseph, K. T. Nguyen, V. M. Murukeshan, S. W. Lye and Y. Zhao, *ChemNanoMat*, 2015, **1**, 39–45.
130 J. H. Park, D. S. Dumani, A. Arsiwala, S. Emelianov and R. S. Kane, *Nanoscale*, 2018, **10**, 15365–15370.
131 A. Welch and S. PimlottIn, PET and SPECT in Drug Development, in *Burger's Medicinal Chemistry and Drug*

Discovery, ed. D. J. Abraham, John Wiley & Sons, Inc., 2010, pp. 737–748, DOI: 10.1002/0471266949.bmc254.
132 S. S. Gambhir, *Nat. Rev. Cancer*, 2002, **2**, 683–693.
133 A. W. Musumeci, T. L. Schiller, Z. P. Xu, R. F. Minchin, D. J. Martin and S. V. Smith, *J. Phys. Chem. C*, 2010, **114**, 734–740.
134 S. Shi, B. C. Fliss, Z. Gu, Y. Zhu, H. Hong, H. F. Valdovinos, R. Hernandez, S. Goel, H. Luo, F. Chen, T. E. Barnhart, R. J. Nickles, Z. P. Xu and W. Cai, *Sci. Rep.*, 2015, **5**, 16930.
135 F. Chen, H. F. Valdovinos, R. Hernandez, S. Goel, T. E. Barnhart and W. Cai, *Acta Pharmacol. Sin.*, 2017, **38**, 907–913.
136 F. Chen, S. Goel, H. F. Valdovinos, H. Luo, R. Hernandez, T. E. Barnhart and W. Cai, *ACS Nano*, 2015, **9**, 7950–7959.
137 S. Eom, G. Choi and J.-H. Choy, *Appl. Clay Sci.*, 2019, **176**, 58–65.
138 A. Campu, M. Focsan, F. Lerouge, R. Borlan, L. Tie, D. Rugina and S. Astilean, *Colloids Surf., B*, 2020, **194**, 111213.
139 S. Rajkumar and M. Prabaharan, *Colloids Surf., B*, 2020, **186**, 110701.
140 Z. Abed, J. Beik, S. Laurent, N. Eslahi, T. Khani, E. S. Davani, H. Ghaznavi and A. Shakeri-Zadeh, *J. Cancer Res. Clin. Oncol.*, 2019, **145**, 1213–1219.
141 H. U. Lee, S. Y. Park, S. C. Lee, S. Choi, S. Seo, H. Kim, J. Won, K. Choi, K. S. Kang, H. G. Park, H. S. Kim, H. R. An, K. H. Jeong, Y. C. Lee and J. Lee, *Small*, 2016, **12**, 214–219.
142 L. Jin, J. Liu, Y. Tang, L. Cao, T. Zhang, Q. Yuan, Y. Wang and H. Zhang, *ACS Appl. Mater. Interfaces*, 2017, **9**, 41648–41658.
143 L. X. Xing, X. Li, Z. H. Xing, F. Li, M. W. Shen, H. Wang, X. Y. Shi and L. F. Du, *Chem. Eng. J.*, 2020, **382**, 122949.
144 Y. Wang, X. Liu, G. Deng, J. Sun, H. Yuan, Q. Li, Q. Wang and J. Lu, *Nanoscale*, 2018, **10**, 2866–2875.
145 X. Li, L. Xing, K. Zheng, P. Wei, L. Du, M. Shen and X. Shi, *ACS Appl. Mater. Interfaces*, 2017, **9**, 5817–5827.
146 Q. Zhao, X. Yi, M. Li, X. Zhong, Q. Shi and K. Yang, *Nanoscale*, 2016, **8**, 13368–13376.
147 Y. Feng, Q. Chen, Q. Yin, G. Pan, Z. Tu and L. Liu, *ACS Appl. Bio Mater.*, 2019, **2**, 747–756.
148 L. Han, J.-M. Xia, X. Hai, Y. Shu, X.-W. Chen and J.-H. Wang, *ACS Appl. Mater. Interfaces*, 2017, **9**, 6941–6949.
149 P. Li, L. Liu, Q. Lu, S. Yang, L. Yang, Y. Cheng, Y. Wang, S. Wang, Y. Song, F. Tan and N. Li, *ACS Appl. Mater. Interfaces*, 2019, **11**, 5771–5781.
150 X. Meng, B. Zhang, Y. Yi, H. Cheng, B. Wang, Y. Liu, T. Gong, W. Yang, Y. Yao, H. Wang and W. Bu, *Nano Lett.*, 2020, **20**, 2522–2529.
151 W. Yang, W. Guo, W. Le, G. Lv, F. Zhang, L. Shi, X. Wang, J. Wang, S. Wang, J. Chang and B. Zhang, *ACS Nano*, 2016, **10**, 10245–10257.
152 S. Sun, J. Chen, K. Jiang, Z. Tang, Y. Wang, Z. Li, C. Liu, A. Wu and H. Lin, *ACS Appl. Mater. Interfaces*, 2019, **11**, 5791–5803.
153 Y. Wang, F. Zhang, H. M. Lin and F. Y. Qu, *ACS Appl. Mater. Interfaces*, 2019, **11**, 43964–43975.
154 D. Jana, S. R. Jia, A. K. Bindra, P. Y. Xing, D. Ding and Y. L. Zhao, *ACS Appl. Mater. Interfaces*, 2020, **12**, 18342–18351.
155 X. X. Wang, D. W. Cao, X. J. Tang, J. J. Yang, D. Y. Jiang, M. Liu, N. Y. He and Z. F. Wang, *ACS Appl. Mater. Interfaces*, 2016, **8**, 19321–19332.
156 H. Zhang, X. T. Tian, Y. Shang, Y. H. Li and X. B. Yin, *ACS Appl. Mater. Interfaces*, 2018, **10**, 28390–28398.
157 Y. Dou, X. Li, W. Yang, Y. Guo, M. Wu, Y. Liu, X. Li, X. Zhang and J. Chang, *ACS Appl. Mater. Interfaces*, 2017, **9**, 1263–1272.
158 C. Zhang, W. Sun, Y. Wang, F. Xu, J. Qu, J. Xia, M. Shen and X. Shi, *ACS Appl. Mater. Interfaces*, 2020, **12**, 9107–9117.
159 X. Peng, R. Wang, T. Wang, W. Yang, H. Wang, W. Gu and L. Ye, *ACS Appl. Mater. Interfaces*, 2018, **10**, 1084–1092.
160 L.-x. Zhang, X.-m. Sun, Z. P. Xu and R.-t. Liu, *ACS Appl. Mater. Interfaces*, 2019, **11**, 35566–35576.
161 P. Zhang, H. Huang, J. Huang, H. Chen, J. Wang, K. Qiu, D. Zhao, L. Ji and H. Chao, *ACS Appl. Mater. Interfaces*, 2015, **7**, 23278–23290.
162 K. Ma, Y. Li, Z. Wang, Y. Chen, X. Zhang, C. Chen, H. Yu, J. Huang, Z. Yang, X. Wang and Z. Wang, *ACS Appl. Mater. Interfaces*, 2019, **11**, 29630–29640.
163 H. Zhang, Y. Wang, H. Zhong, J. Li and C. Ding, *ACS Appl. Bio Mater.*, 2019, **2**, 5012–5020.
164 G. Yang, D. Yang, P. Yang, R. Lv, C. Li, C. Zhong, F. He, S. Gai and J. Lin, *Chem. Mater.*, 2015, **27**, 7957–7968.
165 X. Wu, Y. Zhang, Z. Wang, J. Wu, R. Yan, C. Guo and Y. Jin, *ACS Appl. Bio Mater.*, 2020, **3**, 5813–5823.
166 H. Wang, X. Pan, X. Wang, W. Wang, Z. Huang, K. Gu, S. Liu, F. Zhang, H. Shen, Q. Yuan, J. Ma, W. Yuan and H. Liu, *ACS Nano*, 2020, **14**, 2847–2859.
167 L. León Félix, B. Sanz, V. Sebastián, T. E. Torres, M. H. Sousa, J. A. H. Coaquira, M. R. Ibarra and G. F. Goya, *Sci. Rep.*, 2019, **9**, 4185.
168 A. Indoliya, D. Dhar, M. Mohan and R. Poddar, *J. Magn. Magn. Mater.*, 2020, **514**, 167211.
169 X. Chen, S. Zhu, X. Hu, D. Sun, J. Yang, C. Yang, W. Wu, Y. Li, X. Gu, M. Li, B. Liu, L. Ge, Z. Gu and H. Xu, *Nanoscale*, 2020, **12**, 13637–13653.
170 K. Affram, T. Smith, S. Helsper, J. T. Rosenberg, B. Han, J. Trevino and E. Agyare, *Cancer Nanotechnol.*, 2020, **11**, 5.
171 Y. Dai, C. Wu, S. Wang, Q. Li, M. Zhang, J. Li and K. Xu, *Nanomedicine*, 2018, **14**, 547–555.
172 V. Gulani, F. Calamante, F. G. Shellock, E. Kanal, S. B. Reeder and International Society for Magnetic Resonance in Medicine, *Lancet Neurol.*, 2017, **16**, 564–570.